Optics & Laser Technology 180 (2025) 111464

Contents lists available at ScienceDirect

Optics and Laser Technology

journal homepage: www.elsevier.com/locate/optlastec

Full length article

Pixel intensity optimization and detail-preserving contextual contrast enhancement for underwater images

Bharath Subramani, Magudeeswaran Veluchamy *

Department of Electronics and Communication Engineering, PSNA College of Engineering and Technology, Dindigul, Tamilnadu, India

ARTICLE INFO

Keywords:
Underwater image enhancement
Color compensation
Visibility recovery
Pixel intensity optimization
Image quality assessment

ABSTRACT

Underwater images often suffer from low visibility, serious color cast, and loss of details due to various factors such as light absorption, scattering, and turbidity. In recent years, underwater technology has become increasingly important for application in the fields of marine science and marine engineering. However, underwater image enhancement methods sharpen fine details like edges, contrast, and noise reduction. Vision-based image enhancement methods mainly focus on pixel values, which can result in image artifacts and a lack of fine-tuning capabilities. In this paper, a novel underwater image enhancement method is proposed to address quality degradation issues via color channel correction, texture, and contextual contrast enhancement. The pixel intensity optimization is employed to improve visibility and contrast while restoring the true colors of underwater images. The proposed texture enhancement optimizes the model to produce images with more realistic textures by simultaneously ensuring color consistency. Subsequently, contextual contrast enhancement is used to improve the contrast of the underwater image by enhancing the contrast in localized regions. Extensive evaluation of various datasets show that the proposed method outperforms the state-of-the-art methods in terms of naturalness, visibility, and contrast enhancement of underwater images. Experimental results on several existing underwater datasets demonstrate that the proposed method achieves the best quantitative results compared to other underwater image enhancement methods. The outcomes of different investigations illustrate the efficiency of the proposed method in restoring the high visual quality images while preserving the naturalness and fine details of the underwater scene compared to the other existing enhancement methods. The proposed technique achieves the best values interms of entropy, UIConM, UCIQE, UIQM, PCQI, and BRISQUE metrics of 2463 underwater degraded images obtained from benchmark datasets with different enhancement methods.

1. Introduction

Underwater technology plays a significant role in conducting extensive scientific research, monitoring the environment, and utilizing underwater resources [1]. However, the light scattering and absorption effect of the water bodies can lead to undesirable distortions, such as low contrast, distorted colors, and blurred features in images captured under complex underwater environments. Underwater image enhancement aims to improve the valuable information or local characteristics of the acquired images [2]. To be specific, an inadequate light source reduces the visual quality of the image captured in deep water, making it difficult to emphasize detailed information in the underwater scene. The scattering and absorption of light cause detail blurring and color bias in underwater images. In recent years, numerous methods have been proposed to address the contrast degradation. Contrast-limited adaptive histogram equalization (CLAHE) enhances image contrast through histogram equalization [3,4]. Moreover, enhancement-based methods can directly manipulate image pixel intensities and thus are inefficient in enhancing image quality and improving color bias in underwater scenes. However, they are prone to over-exposure or over-enhancement. Ancuti et al. [5] presented a color balance and fusion (CBF) approach for enhancing underwater images degraded by medium scattering and absorption, which requires no specialized hardware or knowledge of underwater conditions. This technique involves the fusion of two images derived from a color-corrected and white-balanced version of the degraded image to improve edge detection and color contrast. However, this method has limitations in fully restoring colors and achieving natural-looking results. Marques et al. [6] introduced a contrast-guided approach (CGA) to enhance underwater images using local contrast information. This approach is evaluated using the OceanDark dataset,

* Corresponding author.
E-mail addresses: bharath.psna@psnacet.edu.in (B. Subramani), magudeeswaran@psnacet.edu.in (M. Veluchamy).

https://doi.org/10.1016/j.optlastec.2024.111464
Received 17 April 2024; Received in revised form 3 July 2024; Accepted 11 July 2024
Available online 16 July 2024

which significantly improves the visibility of low-light underwater images. However, this method fails to reproduce the original color cast because of the limited information available in complex underwater scenes. Yuan [7] implemented a contour bougie morphology (CBM) based underwater image enhancement method to improve the visual quality affected by medium scattering and light absorption. To highlight rich details, this method employs two structuring elements, roving windows, and multiple morphological operations. The results obtained from the CBM method often have a problem in recovering the complete details of the underwater image. However, this method generates enhanced images with inconsistent color perception. Wu et al. [8] presented a two-stage convolutional neural network (CNN) to effectively improve the quality of degraded underwater images. This network addresses the color distortion, blurred details, and low contrast inherent in underwater images by incorporating structural decomposition. Most experiments concentrate on images acquired near the water's surface, where objects are easily discernible. In comparison, underwater images in shallow depths generally exhibit better clarity than those captured in deep water, where the dense blue-green illumination and scarcity of light sources severely limit visibility. To address these limitations, many researchers have dedicated efforts to improve the visual quality of degraded underwater images and proposed some feasible solutions.

Singh and Bhandari [9] developed a dark image enhancement method using a reflection model and principal component analysis (PCA). This algorithm is used to correct color distortion of dark images through a reflection model, and Fechner principle-based brightness enhancement. The PCA method struggles to produce satisfactory results for underwater images with complex information. Pei and Chen [10] developed a revised underwater dehazing approach to eliminate color correction directly. Multiscale illumination fusion is implemented to reveal more details, making it applicable for underwater detection. Yuan et al. [11] presented a novel underwater image enhancement method that extracts high-quality image textures through multiscale fusion. The texture enhancement-based blurriness and color fusion (TEBCF) method adaptively enhances the contrast to recover visibility, demonstrating impressive contrast, saturation, and sharpness improvements. However, this method overly emphasizes the brightness, resulting in overexposed regions with annoying distortions. Kumar and Bhandari [12] proposed a fuzzy c-means clustering-based image enhancement to address the issue of color detail loss in nearly unseen images. The fuzzy-based contrast enhancement for nearly invisible images (FCENII) approach groups the pixels into clusters and modifies the intensity levels based on membership values to preserve the color and brightness information. This method introduces color distortions, leading to inaccurate representation of colors in the underwater scene. Kumar et al. [13] proposed an auto-color transfer (ACT) method to enhance dark regions of haze images. The scale factors are adaptively selected to dehaze the hazy images captured under different environments. However, this method struggles to accurately restore the original colors due to the complex interactions of the underwater environment. Wang et al. [14] presented a multi-weight and multi-granularity (MWMG) enhancement algorithm to address underwater image degradation due to light scattering. In this approach, color-corrected and contrast-adjusted versions are fused, and it is incorporated with normalized weight maps to attain natural visual quality with even illumination. However, the accuracy of the recovered results heavily depends on precise estimates of the unknown parameters in the underwater imaging model.

Zhang et al. [15] developed a local adaptive contrast enhancement (LACE) scheme to address poor visibility and color distortion of the degraded underwater images. A minimum color cost strategy and a guided fusion are incorporated to reduce color distortion in underwater images. The mean and variance are calculated using the integral maps to regulate the distorted contrast. However, the available color information in the enhanced images is insignificant. Zhang et al. [16] introduced an attenuated color channel correction and detail-preserved contrast enhancement (ACDC) framework to effectively enhance poorly illuminated underwater images. Although the ACDC method is crucial to recover color shifts and overall illumination in underwater images, addressing the loss of image details and edge information caused by scattering remains a challenging task. Dual-histogram-based contrast enhancement and multiscale fusion are incorporated to generate underwater images with better quality. However, the enhanced images affect the overall color appearance and introduce annoying distortion. Zhuang et al. [17] presented a hyper-laplacian reflectance prior (HLRP) based retinex variational framework to enhance the salient structures and fine-scale details of the underwater images. In this method, the extreme brightness improvement in the enhanced images leads to a loss of fine details. Zhou et al. [18] introduced the complementary advantage fusion method as a robust solution for overcoming the quality degradation challenges in underwater images. This approach ensures color fidelity and superior image quality by addressing attenuation through the strategic fusion of global and local contrast-enhancement techniques. Sun et al. [19] developed a novel underwater imaging method that employs a band selection algorithm based on multicriteria decision-making. This system uniquely enhances the image quality while avoiding postprocessing-induced distortion.

Xiao et al. [20] introduced a novel turbid underwater image enhancement method employing parameter-tuned stochastic resonance to address degradation, blurring, and reduced contrast caused by light scattering in turbid water. This framework includes dimensionality reduction and normalization to enhance the weak signals in turbid underwater images. Lu et al. [21] implemented a denoising diffusion probabilistic model to address the challenge of severe color distortions in underwater images. This approach effectively enhances the quality of underwater images by utilizing two U-Net networks and distribution transformations. Zhou et al. [22] developed a complementary advantage fusion method to eliminate the degradation of underwater images captured in an aquatic environment. This method employs double histogram optimization to improve global contrast and utilizes the mean and variance features for local contrast enhancement. Wang et al. [23] introduced an optimal contrast and attenuation difference approach for enhancing underwater images plagued by color casts and blurring caused by complex phenomena. This method employs a two-step approach involving contrast optimization, transmission map refinement, and concealing light estimation. Mainly, enhancement-based methods are employed to address brightness distortion and loss of edge details which are frequently encountered in the processed dim light underwater images. Huang et al. [24] presented a novel zero-reference deep network to address the color attenuation and contrast reduction in underwater images without extensive paired training data. This method employs a lightweight deep network utilizing an underwater curve model to mitigate color dispersion and casting. Zhang et al. [25] developed a transfer-learning-based framework to enhance the underwater images captured by ocean engineering vehicles. This framework addresses low visibility and color distortion issues by transferring in-air image-dehazing techniques. Zhu et al. [26] developed an unsupervised representation disentanglement method to enhance underwater images affected by water medium distortions. This method separates the content and style information to address chromatic aberration, blur, noise, and clarity. Liu et al. [27] implemented a real-time scene recovery framework for restoring degraded images under various weather and imaging conditions, such as underwater, sand dust, and haze. The method utilizes a rank-one prior (ROP) to mathematically characterize the superimposition of a clear image with the same color imaging environment. This method leads to a loss of information in highlights and a lack of balance in the overall brightness distribution of the underwater images. Consequently, an effective underwater image enhancement method is desirable for various complex underwater applications.

Liu et al. [28] designed a grouped color-compensation encoder and channel fusion decoder for underwater image enhancement. This lightweight and scalable deep-learning-based network addresses color

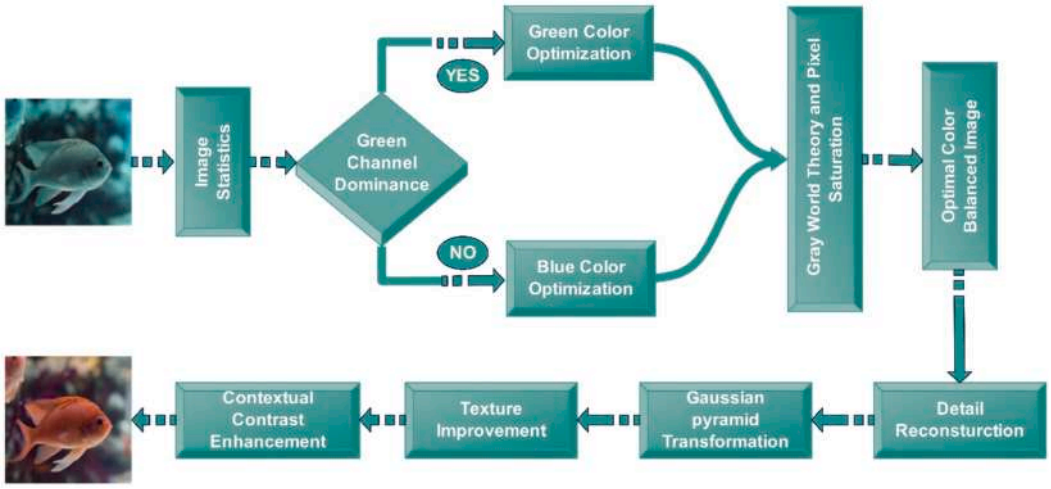

Fig. 1. Process flow diagram of the proposed system.

deviation and low contrast in underwater images. This approach exploits the information-rich green channel and a learnable compensation module to enhance the red and blue channels. Zhang et al. [29] developed a lightweight network for single underwater image enhancement. The depth convolution and one-shot aggregation are implemented to improve the enhancement performance without affecting the running time. Zhang et al. [30] devised a CNN and UNet-based method to enhance the visual quality of the degraded underwater images. This network incorporates a cascade mechanism, information exchange between resolution streams, and a triple-attention module to enhance feature extraction. Yang and Wang [31] proposed an underwater image enhancement method using golden jackal optimization to improve the visibility and quality of underwater images suffering from severe color deviation and low contrast. This algorithm employs a two-stage process. The first stage uses a color compensation and correction strategy to address the color deviation in the RGB color space. The second stage optimizes the image contrast using the golden jackal algorithm. Park and Eom [32] introduced a machine learning-based underwater image enhancement approach by utilizing an adaptive standardization and normalization network. The adaptive standardization network corrects the distorted distribution of the input features, whereas the adaptive normalization network enhances the contrast, removes haze, and restores the mean brightness. Li et al. [33] implemented an adaptive enhancement technique to address the challenges of color distortion and haze in underwater imaging. This method first trains a U-Net network using hue channel statistics for adaptive color correction. Subsequently, a transformer network is trained on hazy terrestrial images to remove haze from the color-corrected underwater images.

An et al. [34] proposed a Hybrid Fusion Method (HFM) to improve the white balance distortion and visibility issues of the underwater images. Type-II fuzzy sets are incorporated to recover the natural visibility and color of the underwater scene. Shen et al. [39] developed a multilevel attention module to improve underwater object detection in complex aquatic environments. This approach includes cross-splitting and cross-linking in the preprocessing and postprocessing stages and adaptive fusion in the attention calibration stage. Shen et al. [40] proposed a multiple information perception-based attention module to enhance underwater object detection in poorly illuminated underwater images. The presented algorithm is integrated into YOLO detectors to improve the detection accuracy significantly. Wang et al. [41] developed an unsupervised hashing algorithm using a graph-collaborated auto-encoder, which effectively learns a unified binary code by collaboratively leveraging low-rank constrained affinity graphs and auto-encoders. The presented method significantly improves the clustering performance on large-scale multiview data. Wang et al. [42] introduced multiview clustering via bi-consistency to address the challenge of clustering unlabeled data with missing instances across multiple views. The system employs bi-consistency guidance with reverse regularization to examine the latent consensus representation and uses manifold embedding to explore hidden structures in the recovered data. The existing methods often lack interpretability and struggle with data dependency and parameter accuracy, making them unsuitable for varied underwater conditions. However, the visual appearance of images captured underwater is always inadequate. They often suffer from severe degradations such as poor contrast, blurred details, and severe color casts due to scattering and light absorption. This imposes several constraints on exploring the underwater environment and subsequent visual perception analysis. Therefore, an efficient technique which can improve underwater images with higher contrast, better clarity, more detail, and extensive colors for both display and analysis is meaningful and thus desired. Besides, state-of-the-art underwater enhancement methods usually fail to restore true colors and lost details simultaneously while enhancing the contrast. Therefore, an effective underwater enhancement method has been developed to address color and white balance degradation, poor perceptibility, and contrast distortion in underwater images. This research aims to improve the underwater image quality, which is often affected by low visibility, serious color cast, and loss of details due to light absorption, scattering, and turbidity. The contributions of this article are summarized as follows: An effective underwater image enhancement method based on color correction and pixel intensity optimization is proposed to reduce color distortion, highlight image details, and improve image visibility. The proposed system method employs Gaussian pyramid transformation to restore blurred details and reveal hidden information in the images. Contextual contrast enhancement is used to improve the contrast in localized regions of the image while restoring their true colors. The proposed method has been extensively evaluated on various underwater datasets, demonstrating superior performance in terms of naturalness, visibility, and contrast enhancement compared to state-of-the-art methods.

The rest of the paper is organized as follows. Section II presents a detailed description of pixel intensity optimization for removing the uneven color cast, Gaussian pyramid transformation to restore blurred details and reveal hidden information, and contextual contrast enhancement to enhance the clarity and sharpness of an underwater image. In Section III, we compare the proposed method with various existing image enhancement techniques, highlighting the strengths and limitations of each approach in addressing color correction, contrast improvement, and detail restoration in underwater images. In section IV, the conclusion will summarize the key findings of the proposed method in enhancing the quality of underwater images.

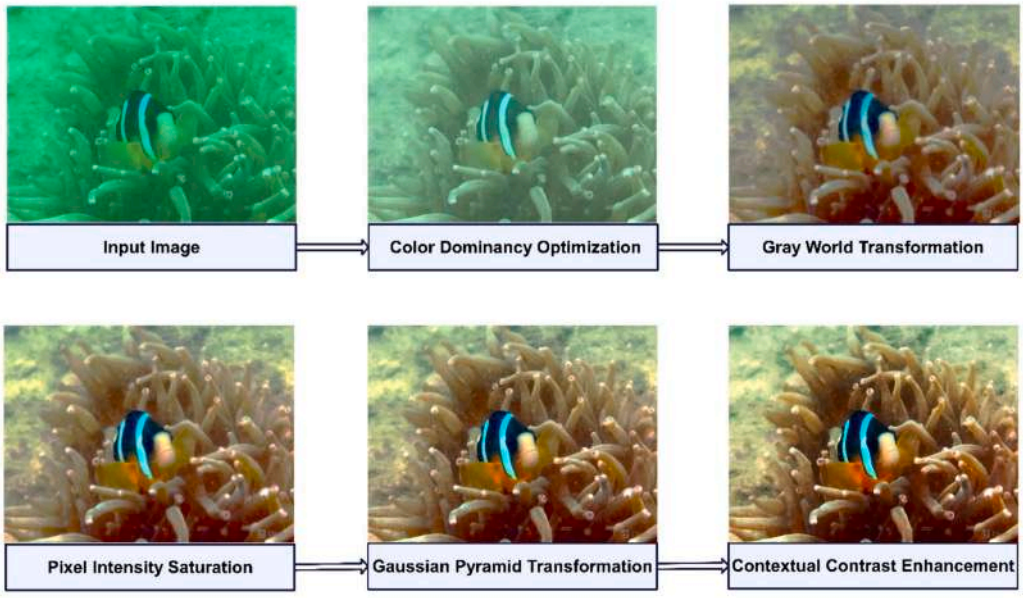

Fig. 2. Schematic workflow diagram of the proposed model.

2. Proposed method

The proposed system is developed to enhance underwater images by addressing the limitations of existing techniques, such as color distortion, low contrast, and detail loss. The process flow diagram of the proposed underwater image enhancement system is depicted in Fig. 1. The proposed system focuses on optimizing pixel intensity and enhancing image texture to improve the quality of underwater images. The proposed method involves statistical analysis of the input image, color channel adjustments based on the dominant channel, and applying the gray world transformation for color balancing. Additionally, Gaussian pyramid transformation is implemented to restore blurred details and enhance visibility. Finally, contextual contrast enhancement is employed to improve the contrast of the underwater image by enhancing it in localized regions. The proposed method mainly focuses on producing color-balanced and detail-rich underwater images, overcoming challenges like color and contrast distortion.

2.1. Pixel intensity optimization

The input image is analyzed statistically to determine the average pixel intensity for each color channel. Let $F(x)$ represent the original image in red, green, and blue (RGB) space with dimensions (i,j) and x corresponds to the spatial location (v,z) in a two-dimensional plane. The input image is defined by,

$$F(x) = \{F^R(x), F^G(x), F^B(x)\} \tag{1}$$

where $F^R(x)$ represents the red plane, $F^G(x)$ represents the green plane and $F^B(x)$ represents the blue plane. The average pixel intensity for each color channel is calculated as,

$$F_a{}^R = \frac{1}{i \times j} \sum_{v=1}^{i} \sum_{z=1}^{j} F^R(v,z) \tag{2}$$

$$F_a{}^G = \frac{1}{i \times j} \sum_{v=1}^{i} \sum_{z=1}^{j} F^G(v,z) \tag{3}$$

$$F_a{}^B = \frac{1}{i \times j} \sum_{v=1}^{i} \sum_{z=1}^{j} F^B(v,z) \tag{4}$$

where $F_a{}^R$, $F_a{}^G$ and $F_a{}^B$ denote the average intensity levels of pixels within the RGB color channels. The channel exhibiting higher average pixel intensity is identified as the dominant channel, while the other two are classified as weaker color channels. The gray world transformation (GWT) [5] is a color-balancing technique that mitigates image color dominance. According to GWT, the average intensity of color channels should appear gray for an image captured in an RGB space under homogeneous lighting conditions. However, in a non-homogeneous environment, the illumination varies, and the images are affected by light scattering and absorption, which leads to color distortion and poor image quality. The GWA often fails to balance images taken in non-homogeneous environments, such as aquatic scenes. Therefore, a pre-processing technique is necessary to adjust the pixel intensity of weaker color channels based on the dominant channel, ensuring a more even distribution of intensity levels. Then, the color correction process is implemented to enhance the pixel intensity of the weaker channels for effective color balancing. The color-balanced image, denoted as $\mathrm{F^P(x)}$, and it is expressed as,

$$F^P(x) = \left(F^{PR}(x), F^{PG}(x), F^{PB}(x)\right) \tag{5}$$

where, $\mathrm{F^{PR}(x)}, \mathrm{F^{PG}(x)}$ and $\mathrm{F^{PB}(x)}$ represents the modified channels of red, green, and blue, respectively. If $\mathrm{F_a{}^G > F_a{}^R}$ and $\mathrm{F_a{}^G > F_a{}^B}$ and $\min\left(\mathrm{F^G(x)}\right) > \min\left(\mathrm{F^R(x)}\right) > \min\left(\mathrm{F^B(x)}\right)$, then the gain factors for the red δ and blue color λ are calculated as follows,

$$\delta = \frac{F_a{}^G}{F_a{}^R} \text{ and } \lambda = \frac{F_a{}^G}{F_a{}^B} \tag{6}$$

The weaker color channels are modified as,

$$F^{PR}(x) = F^R(x) + \frac{\lambda}{\delta} \times \sqrt{\left(F_a{}^G - F_a{}^R\right).\delta + \left(\left(F_a{}^G - F_a{}^B\right)\right)} \tag{7}$$

$$F^{PB}(x) = F^B(x) + \frac{\lambda}{\delta} \times \sqrt{\left(F_a{}^G - F_a{}^B\right).\lambda + \left(\left(F_a{}^G - F_a{}^R\right)\right)} \tag{8}$$

If the $\min\left(\mathrm{F^B(x)}\right) > \min\left(\mathrm{F^R(x)}\right)$, then only the red channel needs to be optimized, and there is no need for the blue channel adjustment. The square root term in the Eqs. (7) and (8) are color dominance reduction factors. When $\mathrm{F_a{}^B > F_a{}^R}$ and $\mathrm{F_a{}^B > F_a{}^G}$, and $\min\left(\mathrm{F^B(x)}\right) > \min\left(\mathrm{F^G(x)}\right)$, then the gain factors for the red δ' and blue color λ' are calculated as

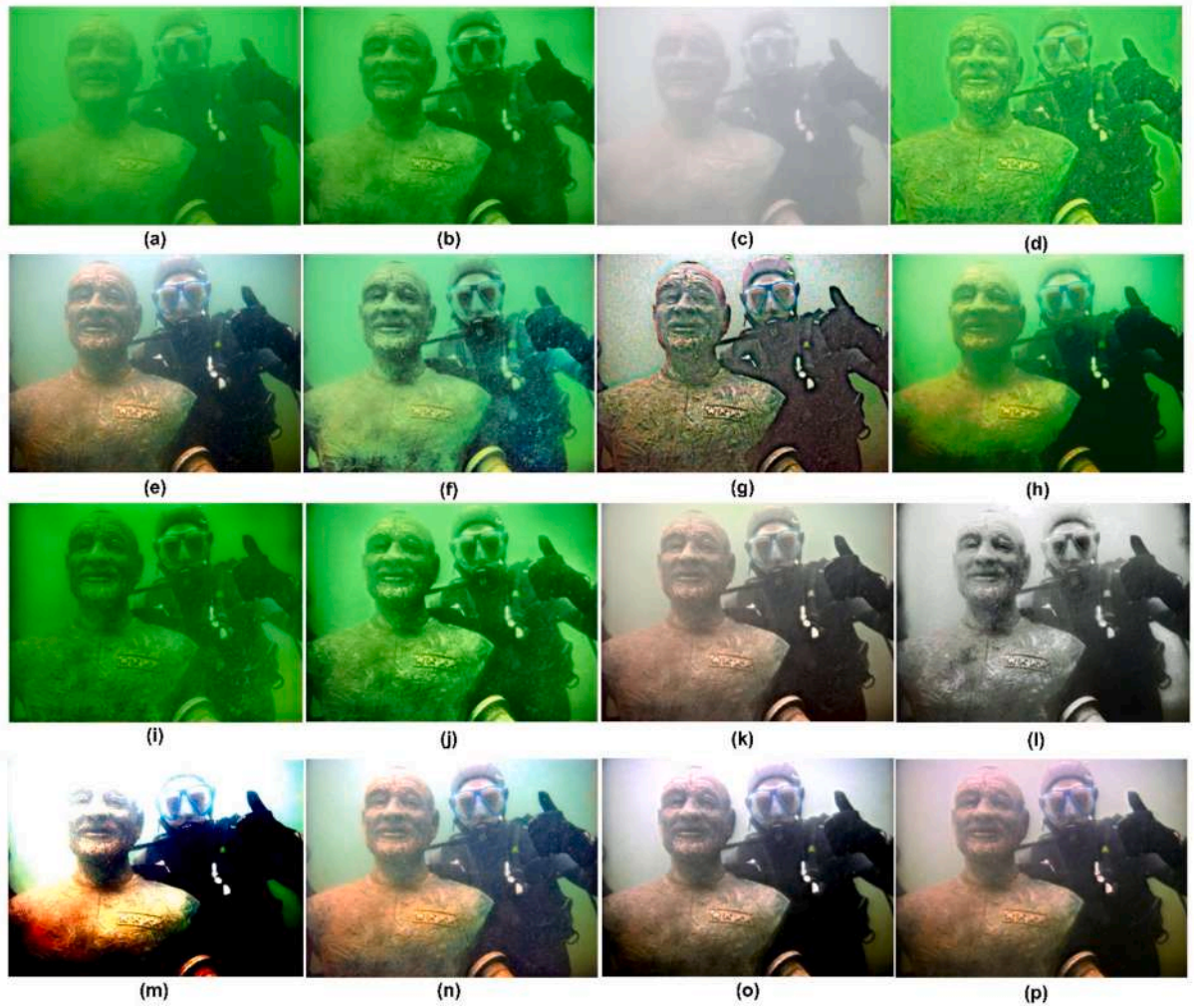

Fig. 3. Assessment of the visual quality and perceptual improvement achieved by various image enhancement techniques on underwater image 1. (a) Original, (b) CLAHE (1987) [3], (c) CBF (2018) [5], (d) CGA (2019) [6], (e) CBM (7) [2021], (f) PCA (9) [2021], (g) TEBCF (2022) [11], (h) FCENII (2022) [12], (i) ACT (2022) [13], (j) MWMG (2022) [14], (k) LACE (2022) [15], (l) ACDC (2022) [16], (m) HLRP (2022) [17], (n) ROP (2023) [27], (o) HFM (2024) [34] and (p) Proposed method.

follows,

$$\delta' = \frac{F_a^{\,B}}{F_a^{\,R}} \text{ and } \lambda' = \frac{F_a^{\,B}}{F_a^{\,G}} \tag{9}$$

The inferior color channels are modified as,

$$F^{PR}(x) = F^{R}(x) + \frac{\lambda'}{\delta'} \times \sqrt{\left(F_a^{\,B} - F_a^{\,R}\right).\delta' + \left(\left(F_a^{\,B} - F_a^{\,G}\right)\right)} \tag{10}$$

$$F^{PG}(x) = F^{G}(x) + \frac{\lambda'}{\delta'} \times \sqrt{\left(F_a^{\,B} - F_a^{\,G}\right).\lambda' + \left(\left(F_a^{\,B} - F_a^{\,R}\right)\right)} \tag{11}$$

If $F_a^{\,G} > F_a^{\,B}$, and $\max(F^{G}(x)) > \max(F^{B}(x))$, then

$$F^{PR}(x) = F^{R}(x) + \sqrt{\left(F_a^{\,G} - F_a^{\,R}\right).\delta + \left(\left(F_a^{\,G} - F_a^{\,B}\right)\right)} \tag{12}$$

$$F^{PB}(x) = \lambda \times F^{B}(x) \tag{14}$$

If $F_a^{\,B} > F_a^{\,G}$, and $\max(F^{B}(x)) > \max(F^{G}(x))$, then

$$F^{PR}(x) = F^{R}(x) + \delta \times \sqrt{\left(F_a^{\,B} - F_a^{\,R}\right).\delta' + \left(\left(F_a^{\,B} - F_a^{\,G}\right)\right)} \tag{15}$$

$$F^{PG}(x) = \lambda' \times F^{G}(x) \tag{16}$$

The lower-intensity pixels of the inferior color channels are adjusted to higher levels, and to preserve the gray-level information, the GWT is applied to the color-balanced version. However, the color-balanced image may exhibit a hazy appearance caused by varying pixel intensities in the foreground and background regions. To mitigate the haze effect, the pixels corresponding to the top and bottom one percent of the intensity levels are saturated across all three color channels.

2.2. Image texture enhancement

The proposed pixel intensity optimization process performs well in color correction but fails to generate an enhanced image with optimized visibility. The Gaussian pyramid transformation is utilized to restore blurred details and reveal hidden information in the color-balanced underwater images. The Gaussian kernel h_l is defined with l different scales and varying window sizes. Then the h_l is convoluted with the color-balanced image F_P to generate l images of the same dimension K_0. Here K_0 signifies the 0^{th} layer of the Gaussian pyramid for 1^{th} iteration. Similarly, to construct the image K_n^l at the n^{th} layer of the Gaussian pyramid for the 1^{th} iteration, we convolve the image K_{n-1}^l from the $n-1^{th}$ layer with the Gaussian kernel h_l. Then, the resulting convolution is subjected to binary extraction in both row and column directions. Mathematically, K_n^l is defined as follows:

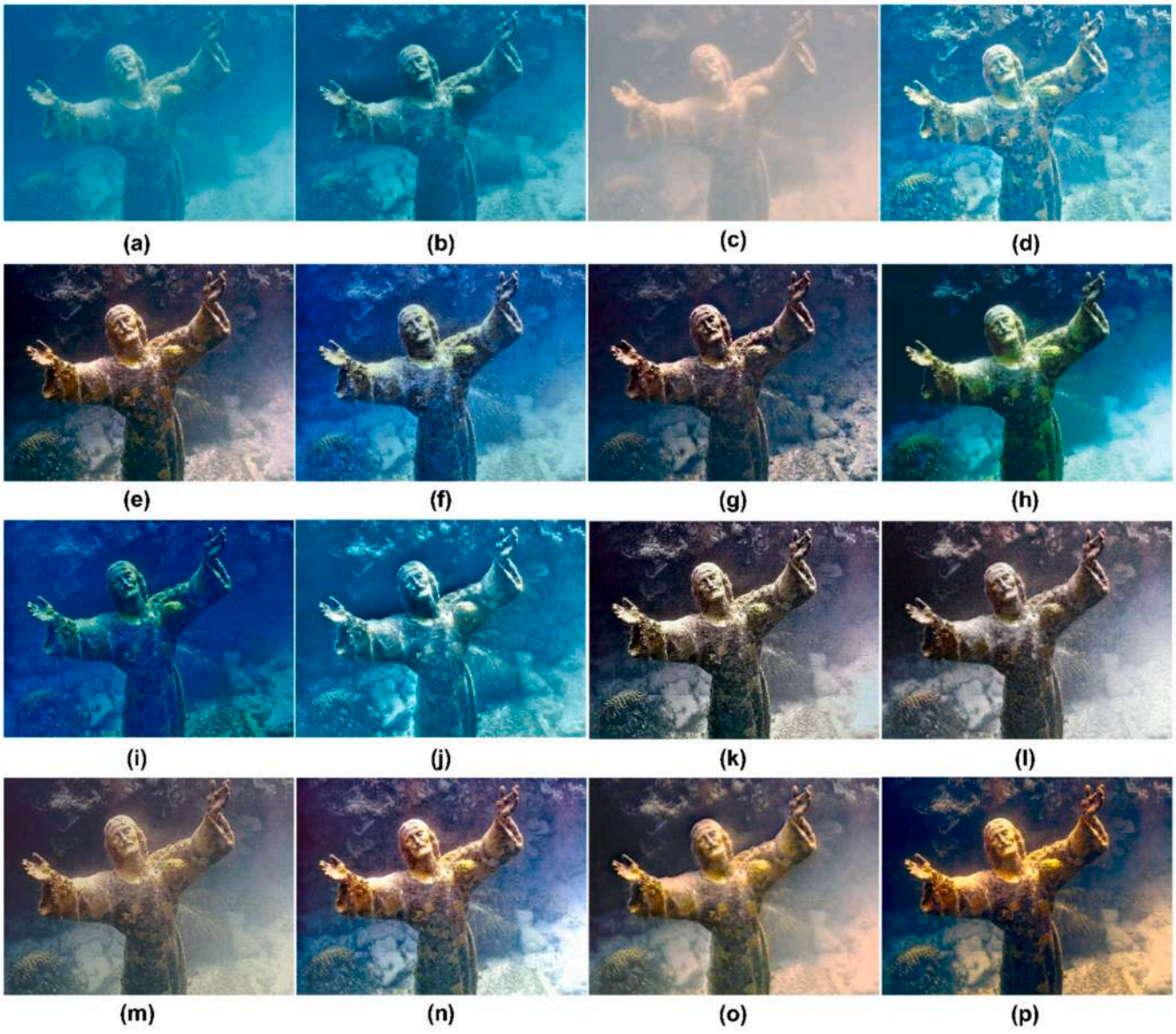

Fig. 4. Assessment of the visual quality and perceptual improvement achieved by various image enhancement techniques on underwater image 2. (a) Original, (b) CLAHE (1987) [3], (c) CBF (2018) [5], (d) CGA (2019) [6], (e) CBM (7) [2021], (f) PCA (9) [2021], (g) TEBCF (2022) [11], (h) FCENII (2022) [12], (i) ACT (2022) [13], (j) MWMG (2022) [14], (k) LACE (2022) [15], (l) ACDC (2022) [16], (m) HLRP (2022) [17], (n) ROP (2023) [27], (o) HFM (2024) [34] and (p) Proposed method.

$$K_n^l(x,y) = \sum_{p_l=-2}^{2} \sum_{q_l=-2}^{2} h_l(p_l, q_l, \sigma_l) K_{n-1}^l(2i + p_l, 2j + q_l) \tag{17}$$

where $(1 \le n \le N, 0 \le x \le R, 0 \le y \le C)$, a Gaussian pyramid with a maximum of N layers, R and C represents the number of rows and columns in the images at the same layer. The size of the image K_n^l in the n^{th} layer of the Gaussian pyramid is reduced by a factor of four compared to K_{n-1}^l. The two Gaussian pyramids K_n^1 and K_n^2 are generated when $l = 2$. Here h_1 denotes the Gaussian kernel with a scale and radius of 3 and h_2 represents the Gaussian kernel with a scale and radius of 5.

The two Gaussian pyramids are denoted as K_n^1 and K_n^2 are obtained through Eq. (17), which has equal layers. The decomposition output yields a high-quality, small-scale image enriched with intricate details. Conversely, the large-scale image enhances contour information significantly while retaining better noise immunity. Integrating the strengths of both scales proves advantageous for preserving detailed features and contour information effectively. Furthermore, the Gaussian differential pyramid is obtained by computing the disparities between consecutive images within each layer of the Gaussian pyramid. The up-sampling process is expressed as,

$$C_n(x,y) = K_n^1(x,y) - K_n^2(x,y) \tag{18}$$

The double up-sampling process from the n^{th} layer to the first layer is computed using Eq. (18). Then, the upsampled images from this layer are added to the layer above, and this process continues until it reaches the 0^{th} layer. The reconstructed image with better details is expressed as,

$$F_R(x,y) = \sum_{n-1} \{ C_{n-1}(x,y) + \bigcup (C_{n-1}(x,y)) \} \tag{19}$$

where the operation $\bigcup(C_{n-1}(x,y))$ corresponds to double up-sampling on the image from the n^{th} layer. Finally, the reconstructed image $F_R(x,y)$ is fused with the color-balanced image $F_P(x,y)$ to obtain the

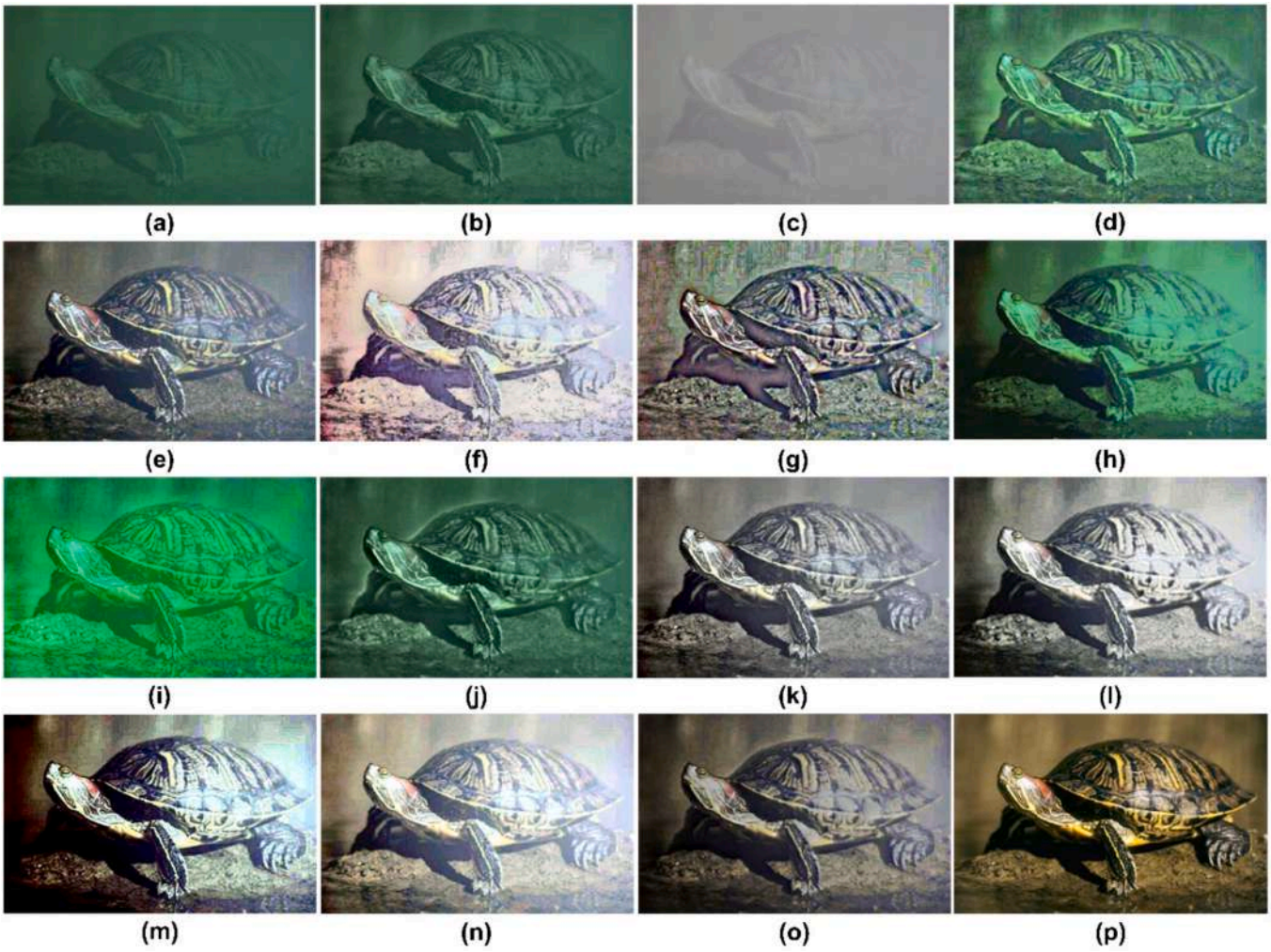

Fig. 5. Assessment of the visual quality and perceptual improvement achieved by various image enhancement techniques on underwater image 3. (a) Original, (b) CLAHE (1987) [3], (c) CBF (2018) [5], (d) CGA (2019) [6], (e) CBM (7) [2021], (f) PCA (9) [2021], (g) TEBCF (2022) [11], (h) FCENII (2022) [12], (i) ACT (2022) [13], (j) MWMG (2022) [14], (k) LACE (2022) [15], (l) ACDC (2022) [16], (m) HLRP (2022) [17], (n) ROP (2023) [27], (o) HFM (2024) [34] and (p) Proposed method.

detail-enhanced underwater image $F_E(x, y)$.

$$F_E(x,y) = F_R(x,y) + F_P(x,y) \tag{20}$$

2.3. Contextual contrast enhancement

The proposed texture enhancement aims to enhance the clarity and sharpness of an image. Conversely, contextual contrast enhancement (CCE) is employed to improve the visual quality of the underwater image by enhancing the contrast in localized regions. CCE operates on new pixel intensities within local areas of the image to achieve a more balanced and visually appealing result. First, the input image is divided into non-overlapping sub-blocks of size M*N. Let B represent the number of sub-blocks. Second, the histogram of each sub-block is calculated, where each histogram represents the distribution of pixel intensities within that sub-block. Let $h_{mn(g)}$ denote the histogram function for the m^{th} and n^{th} sub-block, where g is the gray level. Next, the average pixel count A_P per gray level across all sub-blocks is determined. Then, a clip limit value C_L to restrict the maximum percentage of pixels allowed for each gray level is computed as follows,

$$C_L = A_P{*}\beta \tag{21}$$

where β is the clip coefficient and lies in the range 0 to 1. Next, the gray histogram of each sub-block is clipped, and the clipped pixel counts to each gray level of the histogram are redistributed. Then, Rayleigh distribution is introduced to enhance each clipped histogram, and it is given as,

$$R(x) = R_{min} + \sqrt{2\beta^2 \ln\left(\frac{1}{1 - P_i(x)}\right)} \tag{22}$$

where R_{min} represents the lower limit of the pixel value, and β is a scale parameter. Next, the output of the transformation function is adjusted to reduce abrupt changes in pixel values. Then, local contrast is linearly enhanced based on the transformed values, and it is expressed as,

$$P_O(i) = \frac{T(x) - T_{min}}{T_{max} - T_{min}} \tag{23}$$

where the input parameters for the transformation function are denoted as T(x), T_{max} and T_{min} represents the minimum and maximum values associated with the transformation function. Finally, bilinear interpolation is performed to smooth out pixel values near sub-block boundaries. Interpolated gray value based on neighboring sample points is computed as,

$$I_P(x) = C[dI_{P-}(x) + (1-d)I_{P+-}(x)] + (1-C)[dI_{P-+}(x) + (1-d)I_{P++}(x)] \tag{24}$$

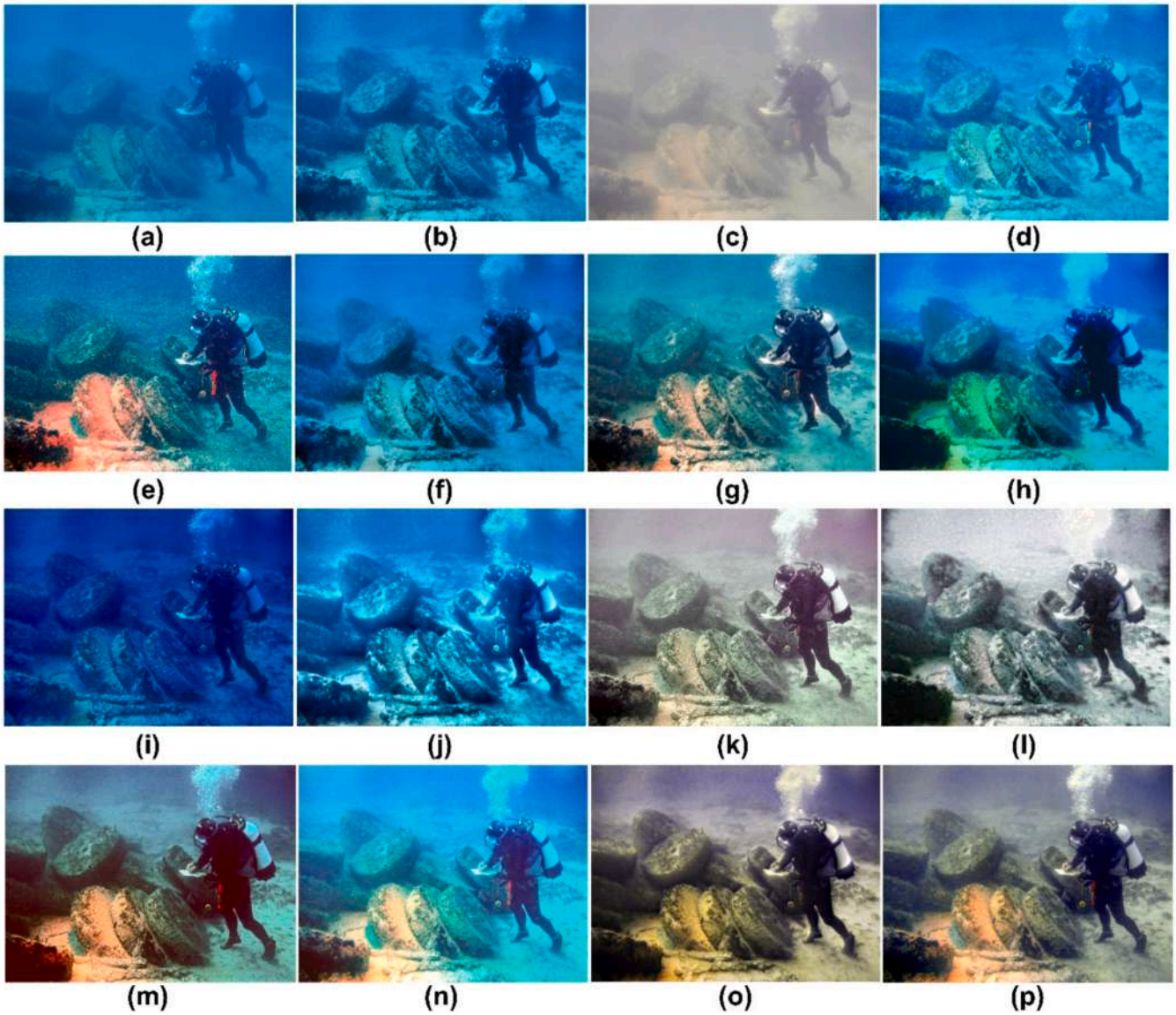

Fig. 6. Assessment of the visual quality and perceptual improvement achieved by various image enhancement techniques on underwater image 4. (a) Original, (b) CLAHE (1987) [3], (c) CBF (2018) [5], (d) CGA (2019) [6], (e) CBM (7) [2021], (f) PCA (9) [2021], (g) TEBCF (2022) [11], (h) FCENII (2022) [12], (i) ACT (2022) [13], (j) MWMG (2022) [14], (k) LACE (2022) [15], (l) ACDC (2022) [16], (m) HLRP (2022) [17], (n) ROP (2023) [27], (o) HFM (2024) [34] and (p) Proposed method.

where I_{P-}, I_{P+-}, I_{P-+}, I_{P++} are the gray level values corresponding to the four different sample points. C and d are the interpolation coefficients that blend the gray values of four sample points around a pixel, resulting in a smoother transition. Fig. 2. represents a schematic workflow diagram of the proposed model. Our proposed method integrates pixel intensity optimization with detail reconstruction and contextual contrast enhancement to comprehensively enhance underwater images. The pixel intensity optimization effectively restores the natural colors of the underwater images. This process adjusts pixel intensities to correct these deviations, ensuring more accurate color representation. The detail reconstruction process is incorporated to address the blurring and loss of detail due to light scattering. The proposed method preserves the textures and fine features of underwater scenes and restores the clarity of fine details often lost in underwater images. Contextual contrast enhancement mainly focuses on improving the contrast of underwater images in localized regions. The CCE targets specific areas of the image that require improvement. The proposed approach effectively enhances the clarity and sharpness of the image while maintaining natural color and avoiding excessive enhancement.

3. Experimental results and discussion

The performance analysis of the different enhancement methods is conducted on the standard benchmark underwater datasets such as Enhancing Underwater Visual Perception (EUVP) [16], Synthetic Underwater Image Dataset (SUID) [27], Underwater Image Dataset (UID) [37], and Underwater Image Enhancement Benchmark (UIEB) [11]. A comprehensive and fair qualitative and quantitative evaluation is conducted using the proposed and recent state-of-the-art methods to assess the enhancement quality of the underwater images. The existing methods used for comparison include CLAHE [3], CBF (2018) [5], CGA (2019) [6], CBM (2021) [7], PCA (2021) [9], TEBCF (2022) [11], FCENII (2022) [12], ACT (2022) [13], MWMG (2022) [14], LACE (2022) [15], ACDC (2022) [16], HLRP (2022) [17], ROP (2023) [27], and HFM (2024) [34].

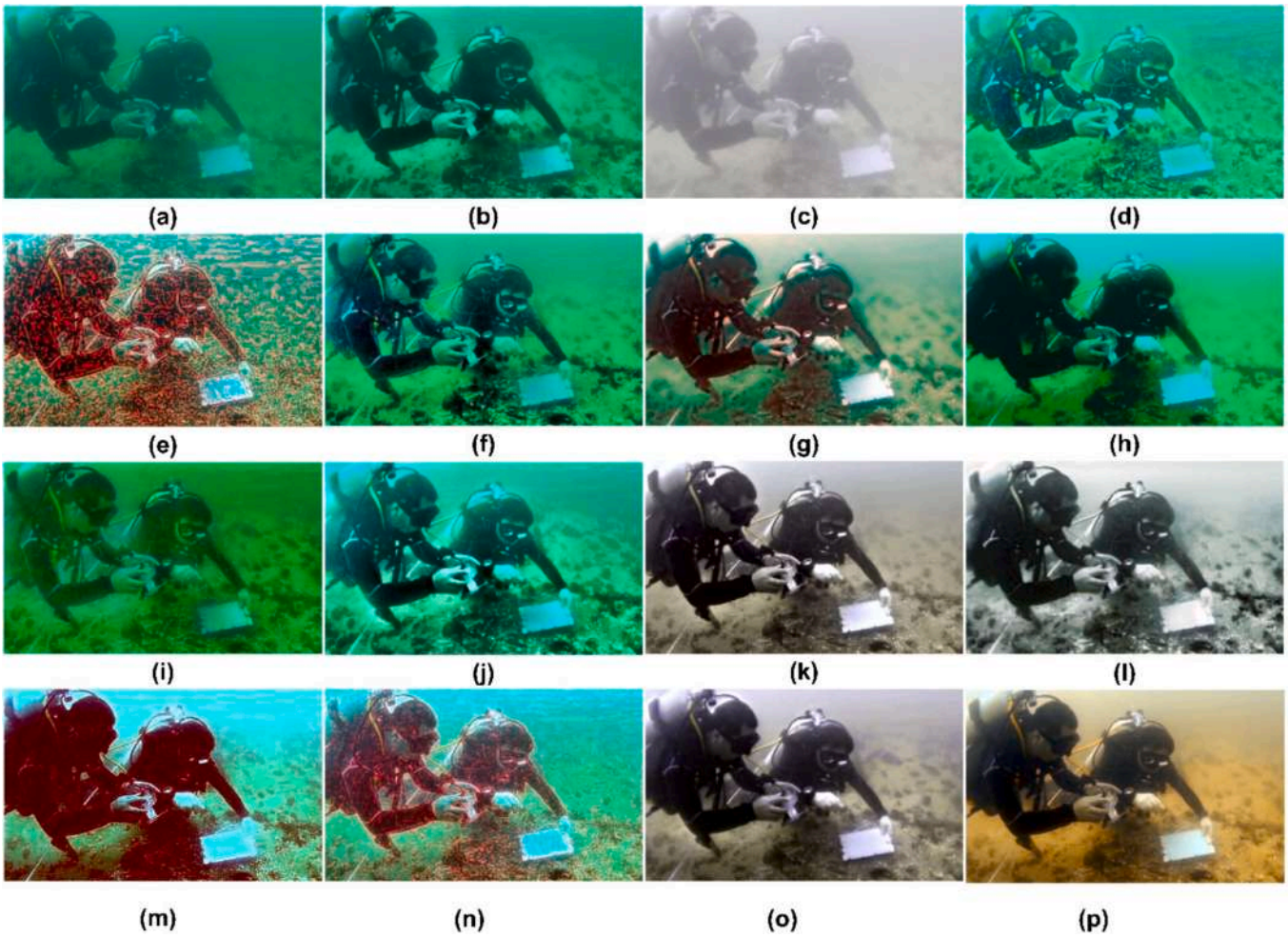

Fig. 7. Assessment of the visual quality and perceptual improvement achieved by various image enhancement techniques on underwater image 5. (a) Original, (b) CLAHE (1987) [3], (c) CBF (2018) [5], (d) CGA (2019) [6], (e) CBM (7) [2021], (f) PCA (9) [2021], (g) TEBCF (2022) [11], (h) FCENII (2022) [12], (i) ACT (2022) [13], (j) MWMG (2022) [14], (k) LACE (2022) [15], (l) ACDC (2022) [16], (m) HLRP (2022) [17], (n) ROP (2023) [27], (o) HFM (2024) [34] and (p) Proposed method.

3.1. Visual quality assessment

The visual quality assessment results on different underwater images are displayed in Figs. 3–11. From Fig. 3, the CLAHE, CGA, PCA, FECNII, ACT, and MWMG methods fail to address the color bias issue, and enhanced images still exhibit unnatural color tones. The CBF method fails to control the brightness during the enhancement process, leading to loss of detail and an unnatural appearance. The CBM method shows insignificant improvement in addressing color deviation and contrast enhancement. The TEBCF approach mainly focuses on enhancing contrast and saturation, which may lead to overexposure and introduce undesirable artifacts in the enhanced images. The LACE method introduces unwanted color distortions and haze-like appearances, making the enhanced image unpleasant. From the results, it is clear that color correction capability of the ACDC method is unsatisfactory, and the enhanced image suffers from a severe over-enhancement problem. The HLRP method fails to restore the actual colors and produces excessive enhancement. The ROP approach enhances the suppressed details but fails to recover the natural color, causing the underwater scene to be over-exposed. The HFM approach shows inconsistencies in color and white balance correction, leading to non-uniform color shifts with detail loss. In contrast, the proposed system achieves accurate and effective color and white balance correction and generates an enhanced image with rich details.

Fig. 4 displays the enhancement results of different methods on underwater image 2. The CLAHE method fails to eliminate the uneven color cast. The CBF method is insignificant in removing the haze effect, and the restored colors are unnatural. The CGA approach generates false textures and also suffers from severe color distortion. The CBM method fails to handle the illumination variation of the underwater scene and yields an image with poor perceptual quality. The actual color of the underwater scene is not reflected in the output of the PCA method. The enhanced image from the TEBCF approach loses its natural appearance while improving the structural information. The FCENII algorithm fails to restore the natural color, edges, and textures of the underwater scenes. The blue bias of the underwater scene is not effectively removed by the ACT method. The performance of the MWMG method in removing color distortion is unsatisfactory. Although the LACE and ACDC approaches can efficiently remove the blue deviation of underwater images, the output images have excessive local enhancement. The enhanced image by the HLRP method lacks sharpness and fails to reveal all structural features. The background of the ROP-enhanced image is dark and indistinct, making it difficult to understand the hidden structural details. The HFM method introduces artifacts and noise that degrade the image quality and distort the natural appearance of the underwater scene. In contrast, the proposed approach achieves better visual sensory results by eliminating color shifts compared to the other existing methods.

Fig. 5 displays the enhancement results of different methods on underwater image 3. The CLAHE method introduces artifacts and noise due

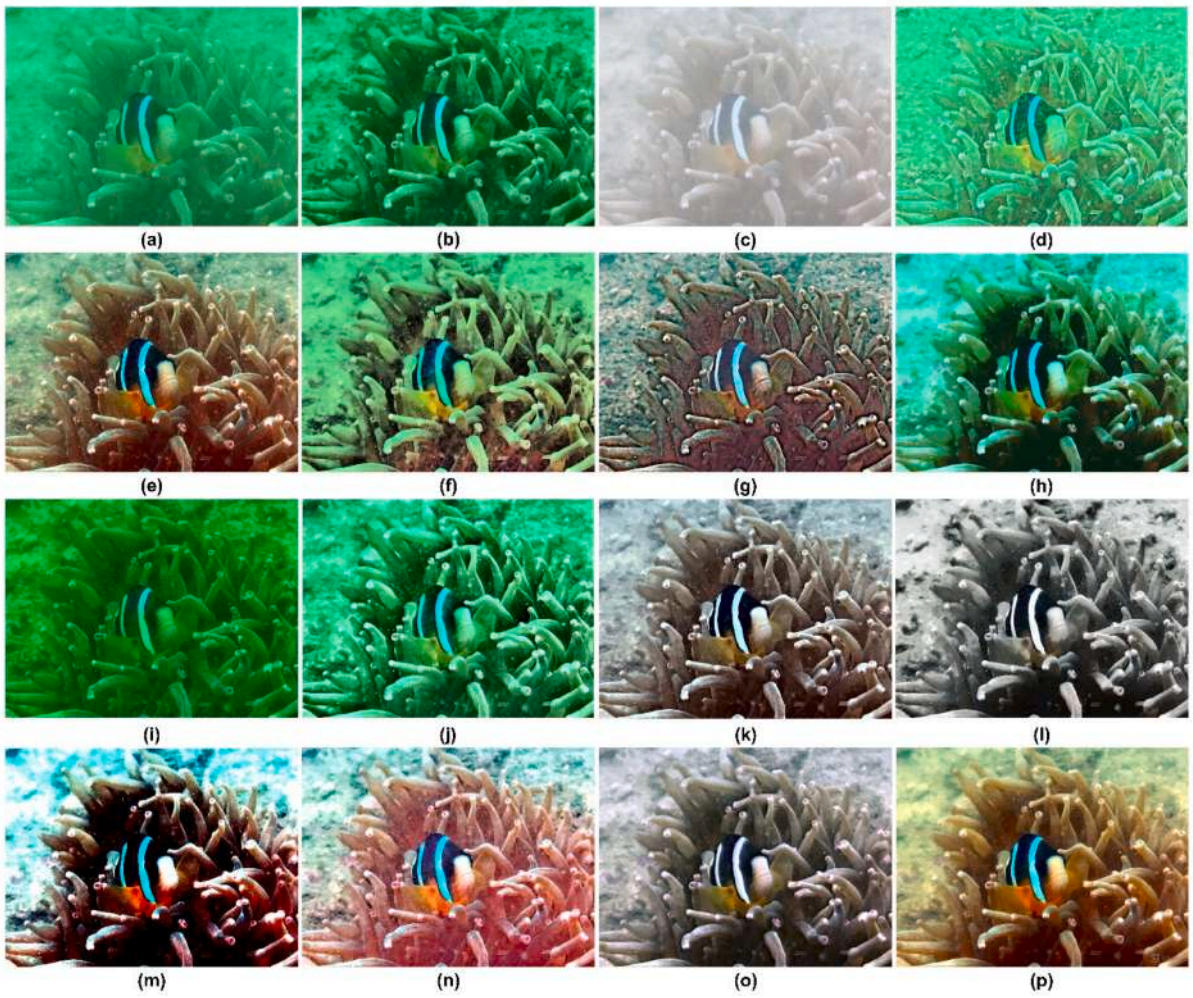

Fig. 8. Assessment of the visual quality and perceptual improvement achieved by various image enhancement techniques on underwater image 6. (a) Original, (b) CLAHE (1987) [3], (c) CBF (2018) [5], (d) CGA (2019) [6], (e) CBM (7) [2021], (f) PCA (9) [2021], (g) TEBCF (2022) [11], (h) FCENII (2022) [12], (i) ACT (2022) [13], (j) MWMG (2022) [14], (k) LACE (2022) [15], (l) ACDC (2022) [16], (m) HLRP (2022) [17], (n) ROP (2023) [27], (o) HFM (2024) [34] and (p) Proposed method.

to aggressive contrast enhancement. The enhanced image by the CBF method has an oversaturation effect and fails to handle all color casts effectively. The CGA method misses subtle details, and the result may not be optimal for all underwater scenes. The enhancement by the CBM method based on context is not accurate. The processed image by the PCA method loses the texture information. The TEBCF method fails to restore the natural color casts. The edge enhancement by the FCENII method is ineffective and contains unnatural sharpness. The ACT method fails to retain the actual colors. Balancing multiple weights by the MWMG method leads to inconsistent results. The LACE method creates uneven exposure on the enhanced image. The color compensation by the ACDC method does not work well in underwater image 3. High-level processing by the HLRP method ignores important low-level details. The ROP method overly processes the input image and loses naturalness. The HFM method results in hyper-realistic images, and it loses its authenticity. In contrast, the proposed method potentially restores natural hues, enhances local contrast and effectively reveals the hidden details without overexposing the image.

Figs. 6–9 illustrate the simulation results of the different methods on four degraded underwater images. The CLAHE method causes over-enhancement, leading to unnatural contrast and noise amplification. The CBF method overcompensates the underwater color cast and produces an image with an unnatural look. The CGA method fails to enhance the local contrast and detail. The CBM method struggles to correct color casts across the entire image in which some areas appear properly balanced while others retain a color tint. The results from the PCA method lead to severe color distortion since it prioritizes variance over color fidelity, which is desirable for accurate color reproduction. The TEBCF method overemphasizes the texture of the input image, which may lead to an unnatural appearance with severe color distortions. The FCENII method enhances contrast but results in over-enhancement and loss of natural appearance. The ACT method struggles to reproduce the original colors accurately. The MWMG method introduces halo artifacts, particularly around the high-contrast edges and complex textures. The LACE method results in uneven illumination, with some areas appearing over-enhanced while others remain under-enhanced. The ACDC method fails to maintain true color fidelity and loses finer details, especially in areas with subtle textures. The HLRP method prioritizes the reflectance over fine details, which leads to a loss of texture and subtle features. The ROP method inadvertently enhances the contrast and details and appears unnatural. The HFM method struggles to maintain consistent image quality. In contrast, the proposed method achieves more natural color tones, better detail preservation, and improved overall image quality.

Fig. 10 illustrates the simulation results of the different methods with the corresponding histogram distribution. The histogram distribution of the original image is positively skewed, with most of the pixel values concentrated on the right side of the histogram. The histogram

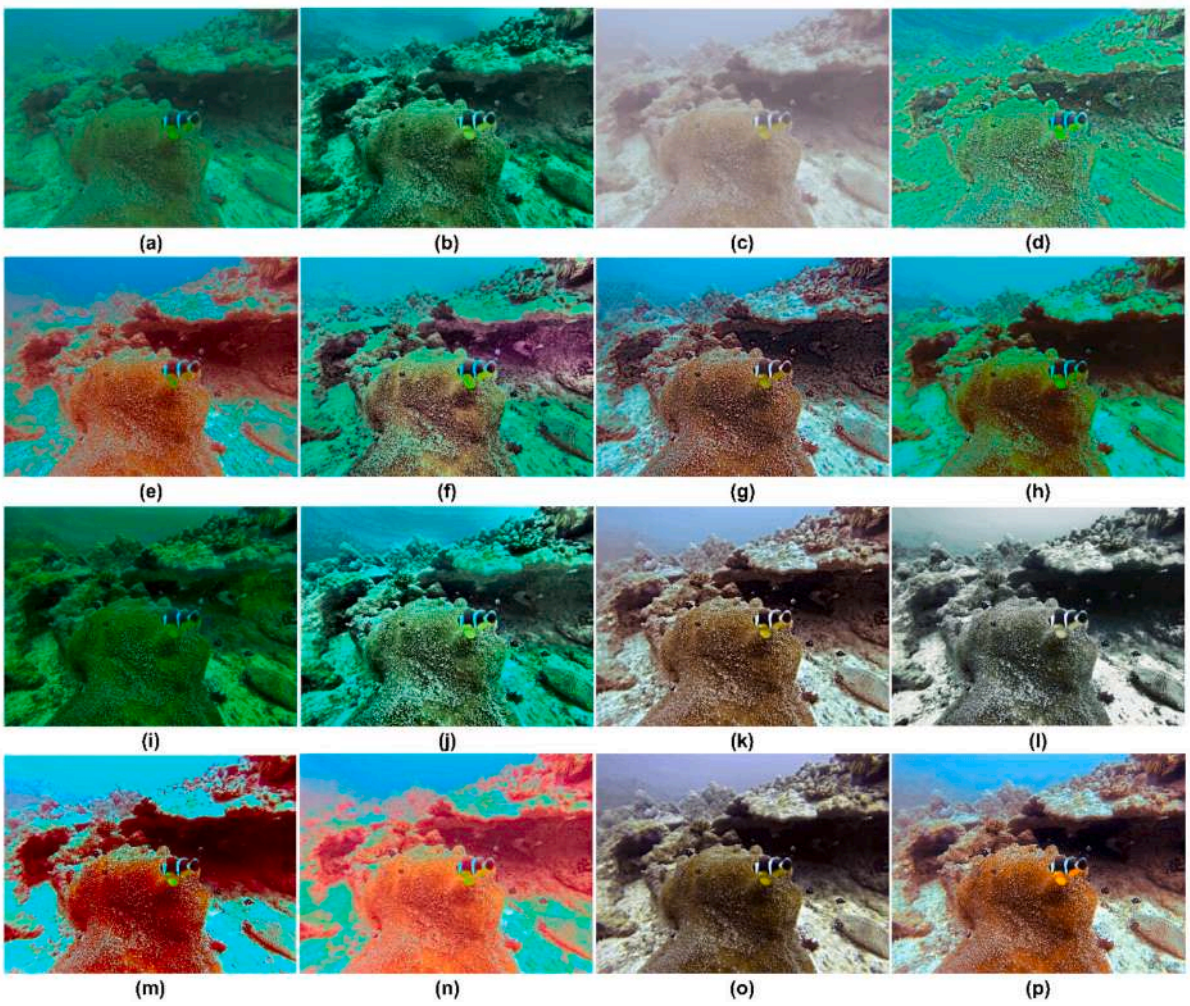

Fig. 9. Assessment of the visual quality and perceptual improvement achieved by various image enhancement techniques on underwater image 7. (a) Original, (b) CLAHE (1987) [3], (c) CBF (2018) [5], (d) CGA (2019) [6], (e) CBM (7) [2021], (f) PCA (9) [2021], (g) TEBCF (2022) [11], (h) FCENII (2022) [12], (i) ACT (2022) [13], (j) MWMG (2022) [14], (k) LACE (2022) [15], (l) ACDC (2022) [16], (m) HLRP (2022) [17], (n) ROP (2023) [27], (o) HFM (2024) [34] and (p) Proposed method.

distribution of the most existing methods is narrow and centered around a low value. Hence, the enhanced images are underexposed and have unclear details and uneven color cast. Meanwhile, the proposed method has a histogram distribution with an expanded dynamic range, which reveals better details and natural colors of the underwater scene. The proposed method is visually compared with other existing methods on five low-quality underwater images with different degradation, as illustrated in Fig. 11. The existing enhancement methods are unsuccessful in color correction and suffer from blur, low contrast, noise, and unclear details. Conversely, the subjective evaluation demonstrates that the proposed method can adjust the color bias of the degraded underwater images and improve the quality of underwater images in challenging environments. Our proposed algorithm significantly addresses the underwater imaging challenges by optimizing pixel intensity for improved visibility, restoring natural colors, enhancing textures to reveal hidden details, and adjusting local pixel intensities for a balanced, visually appealing result. The processed images generated by the proposed algorithm have significant potential for scientific research and monitoring of marine life and environmental changes, analysis of submerged historical sites, and underwater infrastructure inspection, leading to more accurate assessments and timely maintenance.

3.2. Objective assessment

Objective evaluation metrics such as entropy [35,36], underwater image contrast measure (UIConM) [38], underwater color image quality evaluation (UCIQE) [5], underwater image quality measure (UIQM) [5], patch-based contrast quality index (PCQI) [5], and blind/referenceless image spatial quality evaluator (BRISQUE) [13] are employed to measure the quality of enhanced underwater images. Entropy (H) measures the amount of information, clarity, sharpness, and overall fidelity of an image by quantifying the distribution of pixel intensities. Enhanced images with higher entropy values appear visually pleasing due to the richness of detail. Conversely, enhanced images with low entropy values lack visual interest and appear over-smooth. Mathematically, the entropy measure is expressed using Shannon's entropy formula.

$$H(X) = -\sum_{i=1}^{n} p(x_i)\log_2(p(x_i)) \tag{25}$$

where H(X) is the entropy of the image, $p(x_i)$ is the probability of occurrence of pixel intensity x_i, n is the total number of possible pixel intensity values in the image. Table 1 shows that our proposed system demonstrates superior performance in terms of entropy scores compared to other methods. This outcome underscores the effectiveness of our approach in preserving a greater amount of information within the

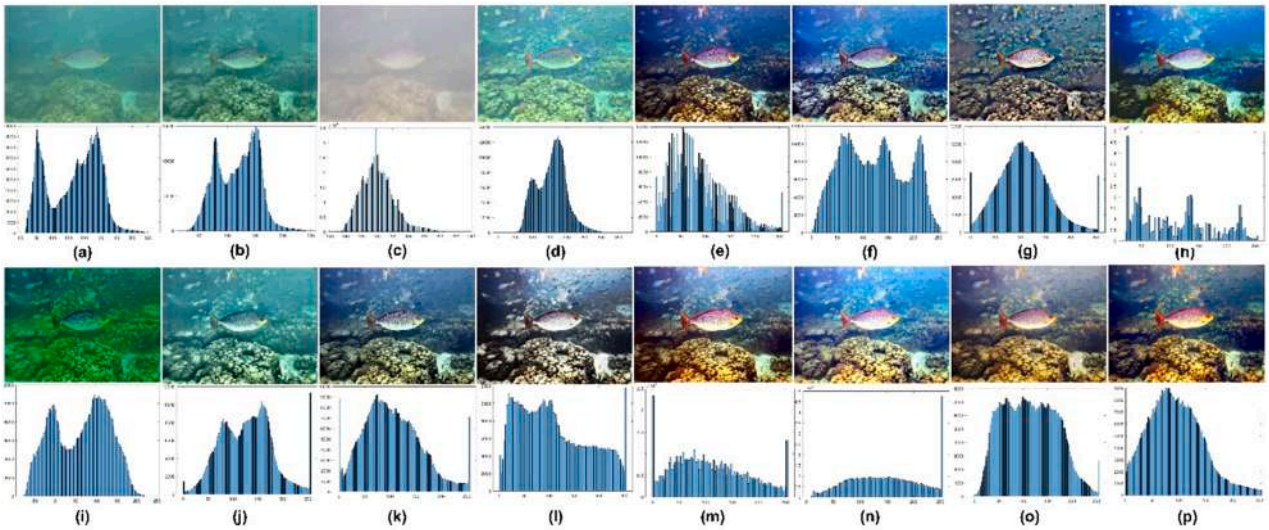

Fig. 10. Assessment of the visual quality and perceptual improvement achieved by various image enhancement techniques on underwater image 8 with its histogram distribution. (a) Original, (b) CLAHE (1987) [3], (c) CBF (2018) [5], (d) CGA (2019) [6], (e) CBM (7) [2021], (f) PCA (9) [2021], (g) TEBCF (2022) [11], (h) FCENII (2022) [12], (i) ACT (2022) [13], (j) MWMG (2022) [14], (k) LACE (2022) [15], (l) ACDC (2022) [16], (m) HLRP (2022) [17], (n) ROP (2023) [27], (o) HFM (2024) [34] and (p) Proposed method.

processed images.

The UIConM metric is computed using logAMEE (logarithmic average Michelson contrast entropy enhancement) operation. This metric introduces the relative contrast ratio within each image block and the average Michelson contrast in local regions. A higher UIConM value indicates a greater contrast, showing clear distinctions between different features in the image. Conversely, a lower UIConM value implies reduced contrast, which may result in poorer image quality. The mathematical expression for UIConM is defined as follows.

$$UIConM = \log AMEE(Intensity) \tag{26}$$

$$\log AMEE = \frac{1}{k_1 k_2}\sum_{l=1}^{k_1}\sum_{k=1}^{k_2}\frac{I_{max,k,l} \ominus I_{min,k,l}}{I_{max,k,l} \oplus I_{min,k,l}} \times \log\left(\frac{I_{max,k,l} \ominus I_{min,k,l}}{I_{max,k,l} \oplus I_{min,k,l}}\right) \tag{27}$$

where $I_{max,k,l}$ and $I_{min,k,l}$ are the maximum and minimum intensity values in each image block, and k_1 and k_2 are the number of blocks in horizontal and vertical directions, respectively.

Table 2 illustrates that the proposed method achieves a higher UIConM value and effectively improves the contrast information of underwater images in global and local regions compared to the other existing methods.

The UCIQE measure quantifies various aspects of image quality, including color fidelity, sharpness, and contrast, which are essential for evaluating the effectiveness of underwater imaging systems. The UCIQE considers the effects of blurring, low contrast, and non-uniform color cast on underwater images. A higher UCIQE value indicates better image quality and reveals accurate color reproduction, sharp details, and adequate contrast in the enhanced underwater image. Conversely, a lower UCIQE value has poor contrast and color distortion. UCIQE of an image is calculated as follows.

$$UCIQE = c_1 \cdot \sigma_{sat} + c_2 \cdot con_l + c_3 \cdot con_{sat} \tag{28}$$

where σ_{sat} is the standard deviation of the saturation channel, con_l is the contrast of the luminance channel, con_{sat} is the contrast of the saturation channel and c_1, c_2, and c_3 are weighting coefficients. According to Table 3, the proposed method attains the highest UCIQE value among all the compared methods. Hence, the proposed system performs best in enhancing the chroma, contrast, and saturation of underwater images.

The UIQM is a no-reference image quality assessment metric used to evaluate the quality of underwater images based on colorfulness, sharpness, and contrast. A higher UIQM value corresponds to a better image quality with vivid colors, clearer edges, and higher contrast. The UIQM score of an image is computed as,

$$UIQM = w_c \times UICM + w_s \times UISM + w_r \times UIConM \tag{29}$$

where w_c, w_s, and w_r are the corresponding weights assigned to balance the overall UIQM score. From the values listed in Table 4, it is understood that the proposed method attains greater UIQM values, and the enhanced images appear more vivid and have more distinguishable bright and dark regions with better contrast.

The PCQI evaluates perceptual distortions in contrast-changed images. PCQI decomposes each image patch into mean intensity, signal strength, and signal structure components and predicts the perceptual quality of contrast variations. Higher PCQI scores indicate better structural preservation and enhancement of contrast. The PCQI is expressed as,

$$PCQI = q_i . q_c . q_s \tag{30}$$

where, q_i denotes the mean intensity difference calculated from the reference and distorted patches, q_c quantifies the contrast change and q_s represents the structural distortion. The test results from Table 5 illustrate that the proposed system gains higher PCQI values than other methods. This higher PCQI value indicates that the proposed system strikes a better balance between enhancing image contrast and minimizing distortions in image structure.

BRISQUE extracts a set of statistical features from the spatial domain of the image and assesses the perceived quality. The statistical properties of the image are distorted by various types of degradation, such as noise, blur, or compression. Smaller BRISQUE scores typically indicate better perceptual quality. The BRISQUE is defined by considering the statistical properties of the mean subtracted contrast normalized (MSCN) coefficients and their pairwise products, and it is modeled using generalized Gaussian distribution (GCD) and asymmetric generalized Gaussian distributions (AGCD).

$$BRISQUE = \sum_{i=1}^{M}\sum_{j=1}^{N}\left[f\left(\frac{\widehat{I(i,j)}}{\alpha}, \sigma^2\right) + \sum_{orientation} f\left(\frac{H(i,j)}{\rho}, {\sigma_l}^2, {\sigma_r}^2\right)\right] \tag{31}$$

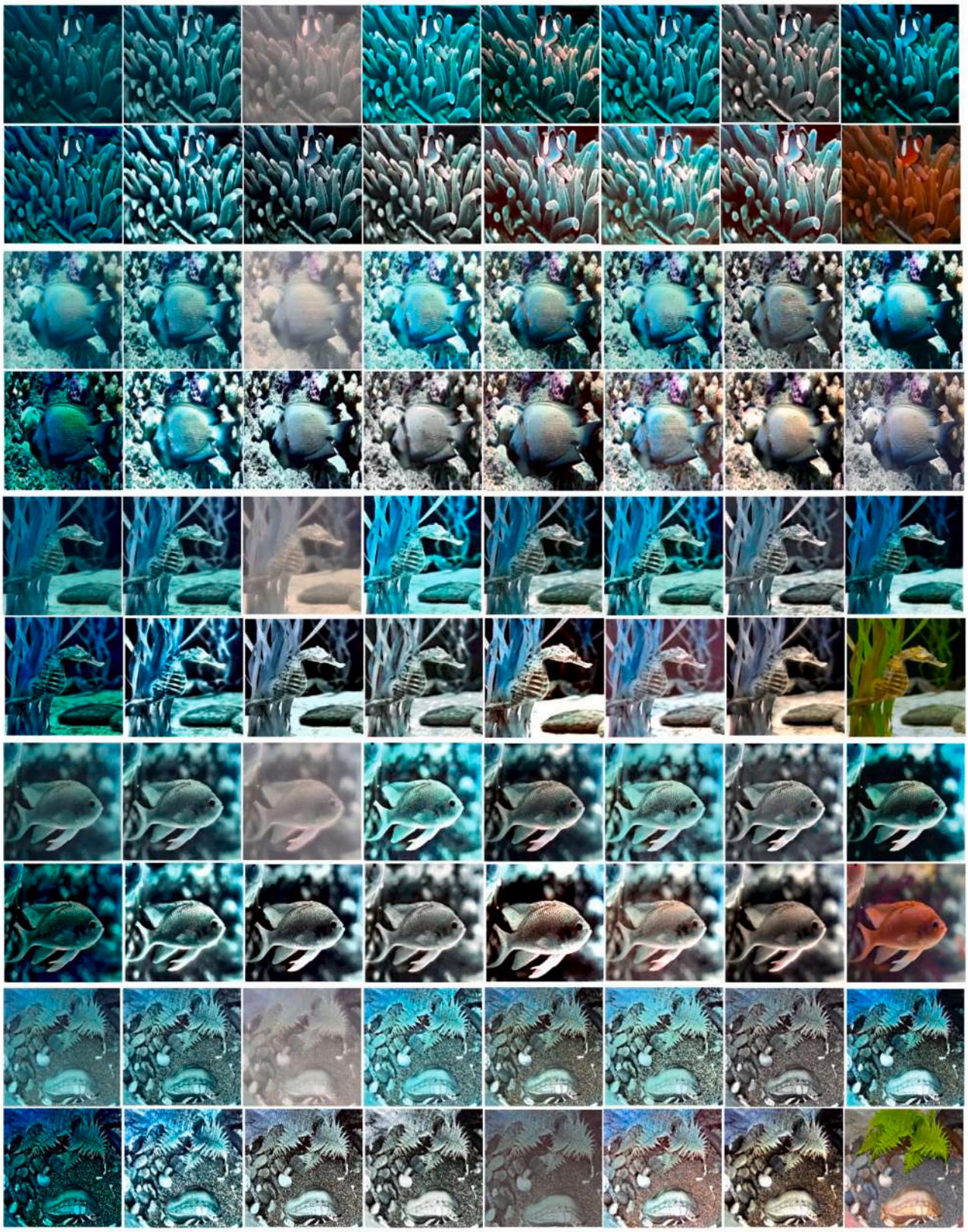

Fig. 11. Assessment of the visual quality and perceptual improvement achieved by various image enhancement techniques on five underwater images. From left to right are the Original, CLAHE (1987) [3], CBF (2018) [5], CGA (2019) [6], CBM (7) [2021], PCA (9) [2021], TEBCF (2022) [11], FCENII (2022) [12], ACT (2022) [13], MWMG (2022) [14], LACE (2022) [15], ACDC (2022) [16], HLRP (2022) [17], ROP (2023) [27], HFM (2024) [34] and the Proposed method.

Table 1
Entropy measurements between the proposed method and the other existing methods.

Methods/Images	1	2	3	4	5	6	7	8	9	10
Original	7.285	7.599	7.741	7.558	7.266	7.637	7.323	7.375	7.528	7.148
CLAHE [3]	7.367	7.622	7.645	7.551	7.711	7.558	7.465	7.472	7.228	6.953
CBF [5]	7.030	6.518	6.949	6.400	6.102	7.357	6.411	6.369	7.120	6.727
CGA [6]	6.229	6.928	7.255	6.353	6.679	6.894	6.358	6.373	5.703	5.585
CBM [7]	7.319	7.502	7.820	7.537	7.047	7.720	7.569	7.484	7.665	7.403
PCA [9]	7.481	7.673	7.772	7.748	7.617	7.926	7.816	7.656	7.691	7.500
TEBCF [11]	7.188	7.836	7.779	7.678	7.762	7.766	7.684	7.644	7.560	7.475
FCENII [12]	6.642	7.180	7.474	7.235	6.863	7.296	7.270	7.220	7.244	7.231
ACT [13]	7.449	7.290	7.553	7.508	7.295	7.441	7.299	7.381	7.190	7.214
MWMG [14]	7.439	7.694	7.561	7.704	7.465	7.603	7.754	7.663	7.608	7.401
LACE [15]	7.533	7.877	7.427	7.804	7.880	7.420	7.666	7.757	7.694	7.338
ACDC [16]	7.625	7.911	7.713	7.801	7.799	7.812	7.800	7.757	7.701	7.657
HLRP [17]	6.961	6.557	5.879	5.574	7.072	7.694	6.395	4.914	3.932	7.423
ROP [27]	7.454	7.716	7.412	7.568	7.596	7.631	7.700	7.626	7.621	7.567
HFM [34]	7.601	7.784	7.796	7.857	7.849	7.631	7.822	7.794	7.759	7.687
Proposed	**7.737**	**7.916**	**7.920**	**7.926**	**7.907**	**7.937**	**7.956**	**7.869**	**7.848**	**7.901**

Table 2
UIConM Measurements Between the Proposed Method and the Other Existing Methods.

Methods/Images	1	2	3	4	5	6	7	8	9	10
Original	0.657	0.485	0.628	0.391	0.557	0.810	0.573	0.531	0.547	0.604
CLAHE [3]	0.432	0.377	0.160	0.289	0.601	0.599	0.467	0.499	0.687	0.792
CBF [5]	0.509	0.274	0.432	0.212	0.223	0.776	0.326	0.261	0.300	0.439
CGA [6]	0.702	0.736	0.629	0.670	0.696	0.847	0.858	0.841	0.778	0.679
CBM [7]	0.691	0.734	0.688	0.695	0.804	0.785	0.798	0.808	0.696	0.762
PCA [9]	0.695	0.717	0.663	0.651	0.798	0.749	0.722	0.807	0.672	0.730
TEBCF [11]	0.746	0.896	0.714	0.770	0.860	0.863	0.856	0.877	0.799	0.868
FCENII [12]	0.638	0.688	0.627	0.576	0.770	0.659	0.738	0.724	0.617	0.735
ACT [13]	0.666	0.693	0.345	0.847	0.332	0.901	0.858	0.447	0.891	0.800
MWMG [14]	0.803	0.770	0.743	0.664	0.737	0.654	0.808	0.808	0.741	0.851
LACE [15]	0.636	0.715	0.483	0.868	0.676	0.709	0.699	0.851	0.659	0.793
ACDC [16]	0.807	0.734	0.714	0.710	0.793	0.823	0.807	0.821	0.685	0.857
HLRP [17]	0.693	0.545	0.357	0.360	0.695	0.978	0.555	0.390	0.290	0.800
ROP [27]	0.809	0.746	0.673	0.709	0.746	0.931	0.788	0.810	0.607	0.767
HFM [34]	0.579	0.652	0.534	0.636	0.683	0.876	0.590	0.754	0.617	0.802
Proposed	**0.924**	**0.900**	**0.889**	**0.910**	**0.890**	**0.942**	**0.912**	**0.886**	**0.901**	**0.913**

Table 3
UCIQE Measurements Between the Proposed Method and the Other Existing Methods.

Methods/Images	1	2	3	4	5	6	7	8	9	10
Original	0.591	0.423	0.574	0.430	0.393	0.605	0.502	0.436	0.565	0.508
CLAHE [3]	0.381	0.482	0.483	0.442	0.460	0.304	0.338	0.490	0.125	0.164
CBF [5]	0.466	0.332	0.432	0.342	0.317	0.503	0.397	0.350	0.450	0.420
CGA [6]	0.357	0.458	0.437	0.477	0.452	0.370	0.321	0.176	0.315	0.370
CBM [7]	0.617	0.628	0.643	0.636	0.672	0.648	0.653	0.644	0.591	0.553
PCA [9]	0.601	0.531	0.609	0.572	0.560	0.630	0.601	0.574	0.581	0.548
TEBCF [11]	0.616	0.617	0.625	0.623	0.662	0.611	0.651	0.629	0.593	0.578
FCENII [12]	0.606	0.576	0.651	0.608	0.574	0.663	0.670	0.593	0.615	0.639
ACT [13]	0.502	0.497	0.574	0.525	0.526	0.501	0.498	0.437	0.512	0.478
MWMG [14]	0.600	0.453	0.605	0.494	0.450	0.652	0.578	0.499	0.595	0.576
LACE [15]	0.601	0.579	0.624	0.605	0.645	0.644	0.638	0.596	0.590	0.556
ACDC [16]	0.625	0.530	0.625	0.541	0.556	0.612	0.601	0.565	0.559	0.555
HLRP [17]	0.669	0.644	0.706	0.679	0.601	0.610	0.610	0.660	0.601	0.599
ROP [27]	0.626	0.638	0.646	0.657	0.669	0.625	0.658	0.639	0.588	0.569
HFM [34]	0.613	0.624	0.679	0.651	0.662	0.680	0.667	0.642	0.602	0.601
Proposed	**0.655**	**0.690**	**0.699**	**0.675**	**0.697**	**0.687**	**0.697**	**0.652**	**0.643**	**0.652**

where $\widehat{I(i,j)}$ is the MSCN coefficient at the pixel (i,j), $H(i,j)$ represents the pairwise product of neighboring MSCN coefficients along different orientations, $f(x,\alpha,\sigma^2)$ denotes the probability density function of the GGD with parameters α and σ^2, $f(x,\rho,{\sigma_l}^2,{\sigma_r}^2)$ represents the probability density function of the AGGD with parameters ρ, ${\sigma_l}^2$ and ${\sigma_r}^2$, M,N are the height and width of the image, respectively. Table 6 shows that the proposed system exhibits smaller BRISQUE values compared to other existing methods. It indicates that the proposed system is more effective in improving images' fidelity and perceptual quality and is more sensitive to subtle distortions and artifacts in images.

Table 7 reports the objective measurement scores of different enhancement methods for an average of 550 underwater images. The results of these comparisons are illustrated as a line plot and displayed in Fig. 12. Overall, the supremacy of the proposed method has been thoroughly verified through various objective measurement metrics. Our method consistently achieves superior values compared to other existing methods. The Proposed and the existing enhancement method was implemented and executed on the personal laptop equipped with the

Table 4
UIQM measurements between the proposed method and the other existing methods.

Methods/Images	1	2	3	4	5	6	7	8	9	10
Original	2.654	0.786	2.134	0.716	0.198	4.181	2.158	1.569	1.814	2.681
CLAHE [3]	4.273	2.225	4.613	4.562	1.775	5.196	7.184	5.887	4.938	5.362
CBF [5]	4.272	3.174	3.788	2.882	2.967	5.268	3.521	3.198	1.497	2.187
CGA [6]	4.502	4.619	4.216	4.337	4.484	5.065	4.998	4.943	5.054	4.890
CBM [7]	3.071	4.216	3.382	3.544	4.313	4.213	3.686	4.597	2.845	3.759
PCA [9]	1.983	2.340	2.796	2.335	2.075	3.576	2.759	3.056	2.201	3.530
TEBCF [11]	4.182	5.041	4.044	4.547	5.226	4.889	4.299	4.871	3.859	4.634
FCENII [12]	3.037	2.709	2.481	2.288	2.679	3.634	3.070	2.966	2.223	3.324
ACT [13]	4.358	4.098	4.534	4.986	6.520	3.158	7.803	4.687	4.333	3.028
MWMG [14]	3.259	1.755	2.627	1.746	0.907	3.804	3.081	2.585	2.867	4.147
LACE [15]	4.576	4.756	2.810	4.803	4.272	4.916	4.182	4.914	3.340	4.300
ACDC [16]	4.255	4.497	4.469	4.470	4.671	4.928	4.308	4.742	3.251	4.437
HLRP [17]	3.362	2.646	1.610	1.830	3.588	5.387	2.493	1.862	1.235	4.160
ROP [27]	4.808	4.504	3.599	3.905	4.467	5.184	3.614	4.541	2.898	3.893
HFM [34]	4.168	4.335	13.971	4.308	4.425	6.010	6.137	4.666	4.744	6.655
Proposed	**5.374**	**5.125**	**5.157**	**4.881**	**7.124**	**6.885**	**7.779**	**7.126**	**6.897**	**7.251**

Table 5
PCQI Measurements between the proposed method and the other existing methods.

Methods/Images	1	2	3	4	5	6	7	8	9	10
CLAHE [3]	0.773	0.612	0.653	0.574	0.603	0.778	0.625	0.690	0.738	0.719
CBF [5]	0.599	0.535	0.779	0.801	0.608	0.760	0.712	0.701	0.718	0.631
CGA [6]	0.267	0.341	0.173	0.265	0.359	0.043	0.248	0.322	0.436	0.276
CBM [7]	1.197	1.252	1.158	1.191	1.195	1.185	1.212	1.297	1.108	1.163
PCA [9]	1.215	1.227	1.043	1.196	1.152	1.100	1.072	1.289	1.011	0.992
TEBCF [11]	1.195	1.429	1.189	1.333	1.247	1.182	1.387	1.263	1.279	1.447
FCENII [12]	0.896	0.991	0.999	1.068	1.012	0.998	1.012	1.050	0.965	1.064
ACT [13]	0.266	0.343	0.170	0.269	0.358	0.043	0.248	0.323	0.437	0.282
MWMG [14]	1.262	1.242	1.146	1.252	1.093	1.237	1.216	1.309	1.158	1.307
LACE [15]	1.151	1.291	1.151	1.268	1.212	1.150	1.259	1.329	1.129	1.292
ACDC [16]	1.140	1.112	1.140	1.130	1.000	1.070	1.035	1.181	1.025	1.178
HLRP [17]	1.122	1.022	1.056	1.153	1.130	1.179	1.005	1.190	1.066	1.163
ROP [27]	1.136	1.240	1.062	1.294	1.169	1.011	1.260	1.320	1.021	1.049
HFM [34]	0.495	0.338	0.495	0.266	0.359	0.040	0.246	0.317	0.434	0.272
Proposed	**1.284**	**1.357**	**1.256**	**1.416**	**1.357**	**1.306**	**1.416**	**1.399**	**1.301**	**1.470**

Table 6
BRISQUE Measurements between the proposed method and the other existing methods.

Methods/Images	1	2	3	4	5	6	7	8	9	10
Original	9.36	17.60	27.72	35.30	20.82	22.38	39.11	41.02	28.22	15.34
CLAHE [3]	9.10	20.88	14.65	26.89	22.85	35.99	35.39	28.02	27.71	21.64
CBF [5]	35.60	40.55	24.47	38.02	25.23	43.46	31.26	38.05	29.02	31.05
CGA [6]	21.59	31.69	23.98	13.36	9.04	33.32	35.47	31.46	23.42	17.10
CBM [7]	31.04	32.85	28.82	9.19	26.49	43.46	31.91	32.82	20.34	14.98
PCA [9]	17.59	19.42	16.09	28.14	11.16	35.45	31.67	24.70	18.83	11.12
TEBCF [11]	24.23	39.26	26.21	40.45	28.77	33.01	35.39	42.20	24.09	19.30
FCENII [12]	24.01	20.91	28.20	25.52	24.35	17.48	30.97	30.21	26.29	17.14
ACT [13]	31.50	25.76	6.92	23.31	13.34	25.51	33.28	38.98	21.20	7.00
MWMG [14]	19.29	30.90	28.03	8.97	26.52	43.41	38.92	23.69	22.29	20.37
LACE [15]	15.69	40.14	15.69	25.67	34.39	22.19	18.49	13.63	24.43	29.00
ACDC [16]	32.53	14.14	32.53	14.46	9.29	33.17	35.54	29.70	31.24	24.74
HLRP [17]	19.65	35.89	19.65	30.42	22.89	43.46	28.23	42.54	41.19	31.88
ROP [27]	25.91	25.48	12.60	21.79	23.67	33.51	33.99	30.47	32.93	14.65
HFM [34]	27.71	16.89	27.71	27.41	4.26	29.08	30.81	34.73	19.56	16.02
Proposed	**8.59**	**14.25**	**10.23**	**12.53**	**8.24**	**14.24**	**18.26**	**19.27**	**16.60**	**5.70**

12th Gen Intel(R) Core(TM) i7-1260P processor running at 2.10 GHz, 16 GB of memory, and MATLAB 2021b. The processing times of various underwater image enhancement methods are assessed, and the runtime results are summarized in Table 7. The proposed method generally exhibits faster processing speeds compared to recent methods. The proposed system optimizes the pixel intensity and enhances the texture to improve underwater image quality using statistical analysis, color channel adjustments, gray world transformation, Gaussian pyramid transformation, and contextual contrast enhancement. The proposed method aims to produce color-balanced, detail-rich images by addressing color and contrast distortion issues. The proposed method shows promising results in enhancing underwater images. However, the current implementation may not be optimized for real-time processing.

To provide a fair and comprehensive assessment of our method, we have conducted an objective evaluation on the entire EUVP (613 underwater images), SUID (900 synthetic underwater images), UID (60 multiply degraded underwater images), and UIEB (890 degraded underwater images) datasets. Table 8 shows that the proposed method attains an optimal image quality assessment score compared to existing approaches. The entropy measurements on all four datasets indicate that

Table 7
Objective measurements between the proposed method and the other existing methods on an average of 550 underwater images.

Methods/Measures	ENT	UIConM	UIQM	UCIQE	PCQI	BRISQUE	Time Cost (s)
Original	7.236	0.547	1.798	0.517	–	24.714	–
CLAHE [3]	7.457	0.490	4.901	0.367	0.684	24.117	0.5772
CBF [5]	6.325	0.287	3.541	0.412	0.675	32.530	9.247
CGA [6]	6.1332	0.618	4.972	0.328	0.262	23.07	41.271
CBM [7]	7.186	0.613	3.762	0.658	1.172	26.878	2.791
PCA [9]	7.451	0.632	2.682	0.5733	1.173	20.451	1.2743
TEBCF [11]	7.238	0.702	4.5017	0.629	1.227	31.547	14.537
FCENII [12]	6.922	0.573	2.103	0.626	1.042	24.537	0.2125
ACT [13]	7.108	0.575	4.762	0.525	0.343	21.647	2.941
MWMG [14]	7.136	0.673	2.781	0.558	1.234	25.125	2.7782
LACE [15]	7.341	0.712	4.635	0.671	1.258	22.478	1.2144
ACDC [16]	7.554	0.7854	4.453	0.561	1.152	24.767	3.154
HLRP [17]	6.042	0.548	2.767	0.643	1.172	30.587	**0.0447**
ROP [27]	7.054	0.779	4.152	0.641	1.212	24.812	4.989
HFM [34]	7.729	0.668	5.782	0.645	0.334	22.478	4.998
Proposed	**7.805**	**0.902**	**6.452**	**0.684**	**1.371**	**12.744**	1.1015

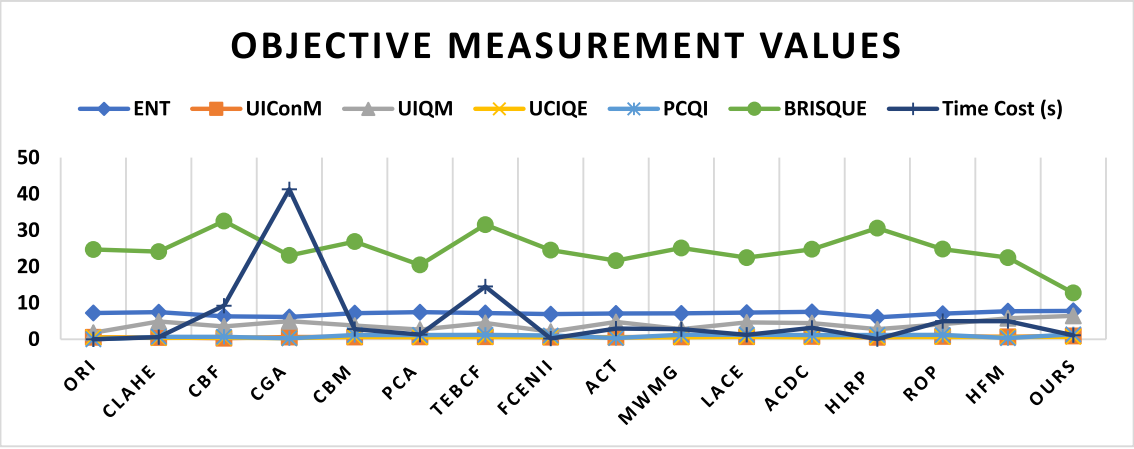

Fig. 12. Line plot representing the objective measurement values by the various underwater enhancement methods.

the proposed method preserves more information and effectively enhances the clarity, sharpness, and overall fidelity of underwater images. The UIConM metric assesses the enhancement of contrast information in global and local regions. The higher UIConM values achieved by the proposed method on all four databases demonstrate its effectiveness in improving the contrast of underwater images. The proposed method's superior UCIQE scores indicate that the processed image contains accurate color reproduction, sharp details, and adequate contrast. The higher UIQM values in Table 7 show that the proposed method generates enhanced images with more vivid colors and better-defined bright and dark regions, contributing to a more pleasant visual experience. The proposed method attains a higher PCQI score and strikes a perfect balance between enhancing contrast and maintaining the structural integrity of the image. The BRISQUE scores of the proposed method are lower when compared to other approaches and indicate that it is more effective in improving the perceptual quality of images and is sensitive to subtle distortions.

3.3. Ablation study

To validate the effectiveness of the presented method, an ablation study was conducted on the four degraded underwater images, and the results are presented in Fig. 13 and Table 7. The contribution of each component in our underwater image enhancement framework is validated. The presented underwater image enhancement framework includes five key elements such as color dominancy optimization (CDO), gray world theory (GWT), pixel intensity saturation (PIS), Gaussian pyramid transformation (GPT), and contextual contrast enhancement (CCE). On visual assessment, it is observed that the proposed CDO fails to achieve a balance between contrast, color, and detail enhancement. The proposed CDO+GWT struggles to correct color casts, leading to an unnatural look. The enhanced image by the proposed CDO+GWT+PIS has a potential loss in fine details and contrast. Detail boosting by the proposed CDO+GWT+PIS+GPT leads to an unnatural contrast and edge definition. In comparison, the proposed CDO+GWT+PIS+GPT+CCE balances color correction and contrast enhancement and generates an enhanced image with rich details.

Table 9 reports the objective measurements of different components of the proposed method on four underwater images. The best results are indicated in bold. After incorporating each component, the objective scores of the test image increase to varying degrees. The + CDO method has a significant impact on improving UIQM and BRISQUE scores. The + GWT potentially increases the UCIQE score. The BRISQUE score of the + PIS method drops slightly and obtains good quality. The + CDO, +GWT, and + PIS methods have little impact on the increasing entropy score. The + GPT significantly improves overall objective scores. However, the enhanced image appears to have poor contrast. The + CCE approach obtains a higher objective score when compared to all methods and generates an image with improved detail preservation and enhanced textures.

4. Conclusion

This paper presents an effective method based on color correction

Table 8
Objective measurements between the proposed method and the other existing methods on four datasets.

EUVP Dataset								SUID Dataset						
Methods/ Measures	**ENT**	**UIConM**	**UIQM**	**UCIQE**	**PCQI**	**BRISQUE**	**Time (s)**	**ENT**	**UIConM**	**UIQM**	**UCIQE**	**PCQI**	**BRISQUE**	**Time (s)**
Input	7.3823	0.8240	3.9137	0.5931	–	42.3610	–	7.4147	0.6341	2.3073	0.5238	–	28.6643	–
CLAHE	7.3388	3.1958	3.3481	0.5740	0.8505	42.5722	0.1558	7.5810	0.8122	5.4703	0.6358	0.8002	19.3683	0.2074
CBF	7.0679	0.6145	4.2772	0.4767	0.6907	32.9897	1.3932	6.4655	0.5494	4.1173	0.3861	0.7329	30.5544	2.6720
CGA	6.9596	0.8251	4.8673	0.3846	0.2275	45.1570	3.1487	6.9465	0.8947	5.4720	0.3979	0.1652	20.6500	8.4826
CBM	7.5108	0.8255	4.6574	0.6365	1.1325	44.3125	0.4241	7.5025	0.6035	4.3956	0.6257	1.2218	16.5201	0.7389
PCA	7.7852	0.8264	3.9098	0.6117	1.1099	45.9284	0.3919	7.7436	0.5396	2.0177	0.5666	1.1383	19.6596	0.6176
TEBCF	7.4261	0.7449	4.6127	0.6107	1.0719	40.3818	0.9741	7.6884	0.6893	4.6014	0.5846	1.2365	20.1923	2.9321
FCENII	6.9580	0.7364	3.8498	0.6596	1.0348	34.6235	0.0446	7.2961	0.5146	2.0754	0.6282	1.0742	32.1390	0.0786
ACT	7.4194	0.8213	4.0071	0.5875	0.2274	42.2414	0.2653	7.3642	0.4998	4.0582	0.5749	0.1635	20.2211	0.7415
MWMG	6.1881	1.3165	5.7955	0.6541	0.9319	51.1336	0.3600	7.5330	0.5996	2.2526	0.5941	1.1067	24.1908	0.6709
LACE	7.1125	0.8428	5.3333	0.5913	1.0938	38.3695	0.1166	7.5789	0.4419	3.3333	0.5729	1.2458	21.5885	0.2707
ACDC	7.7795	0.8582	4.9188	0.5798	0.9977	45.6223	0.2872	7.5267	0.6132	3.8114	0.5781	1.0902	23.9388	0.8137
HLRP	5.9104	0.5197	2.7077	0.6374	1.1478	36.5192	**0.0048**	7.6242	0.6625	3.8749	0.5881	1.1087	31.3428	**0.0121**
ROP	7.5848	0.8233	5.1219	0.6322	1.0082	46.6677	0.4677	7.6330	0.7030	4.3399	0.6001	1.0628	33.8262	1.2267
HFM	7.5116	0.8230	4.8239	0.4979	0.2262	44.6018	0.7550	7.7318	0.4498	3.6652	0.4880	0.1617	31.1015	1.4640
Ours	**7.8123**	**0.9197**	**6.4578**	**0.6759**	**1.2058**	**30.1479**	1.0216	**7.8012**	**0.9015**	**6.2476**	**0.6687**	**1.2569**	**15.2479**	1.1562
UID Dataset								**UIEB Dataset**						
Input	7.7905	0.6742	2.7441	0.5043	–	18.0486	–	6.7010	0.2966	1.0561	0.4532	–	40.6348	–
CLAHE	7.5988	0.4123	3.4398	0.5801	0.7214	31.6239	0.1872	7.6814	0.5756	3.1397	0.6044	0.6798	26.5885	0.2644
CBF	6.8528	0.4847	3.9625	0.4198	0.6557	43.4581	2.5549	6.5679	0.1846	2.7595	0.3421	0.7261	48.7224	4.2255
CGA	6.8820	0.6323	4.3346	0.4889	0.1859	28.7578	8.6466	6.5945	0.5069	5.5864	0.3183	0.4136	15.6467	40.6874
CBM	7.6803	0.7870	4.4916	0.6465	1.2501	41.5317	3.5393	6.5422	0.5624	3.9146	0.6364	0.9964	43.4582	6.3342
PCA	7.9129	0.7574	3.5454	0.6097	1.2440	32.4155	2.3562	7.2869	0.5019	4.4206	0.5517	1.2058	19.1122	3.6823
TEBCF	7.5032	0.8207	4.5999	0.6261	1.2665	25.2503	9.0764	7.7837	0.6245	3.4940	0.6179	1.1270	28.5947	17.1978
FCENII	7.4266	0.7156	3.4520	0.6500	0.9891	19.0382	0.2699	6.2846	0.5964	0.1567	0.5971	0.9967	33.6197	0.3779
ACT	7.5280	8.3391	3.9020	0.6071	0.1792	22.5807	0.6525	7.4061	0.5063	5.5152	0.5306	0.4166	28.7819	3.0723
MWMG	7.5426	0.8213	3.2625	0.6080	1.1810	30.6276	2.0652	7.3284	0.6261	3.1033	0.5543	1.1010	29.6264	2.7073
LACE	7.7552	0.8436	4.9289	0.5946	1.2729	28.7476	0.7392	7.7713	0.6142	4.3566	0.5803	1.1478	26.6684	1.0935
ACDC	7.7309	0.8277	4.9606	0.5606	1.1416	20.7540	0.7572	7.7343	0.6762	4.1470	0.5312	1.0959	31.1176	3.8185
HLRP	7.4865	0.7151	3.9819	0.6516	1.1069	43.4189	**0.0259**	5.9793	0.5280	2.3282	0.7157	1.1279	27.8087	**0.0453**
ROP	7.5683	0.8594	4.9333	0.6501	1.3138	29.1254	2.6806	7.6337	0.6783	2.9430	0.6548	1.0585	43.4582	4.7750
HFM	7.8058	0.8609	5.3086	0.6418	0.1817	16.7749	1.4322	7.4865	0.6362	4.2705	0.6507	0.4143	34.9561	6.2950
Ours	**7.8296**	**0.8976**	**5.9987**	**0.6748**	**1.3254**	**15.4789**	1.1326	**7.7985**	**0.8906**	**5.5998**	**0.6851**	**1.3058**	**15.0697**	1.5479

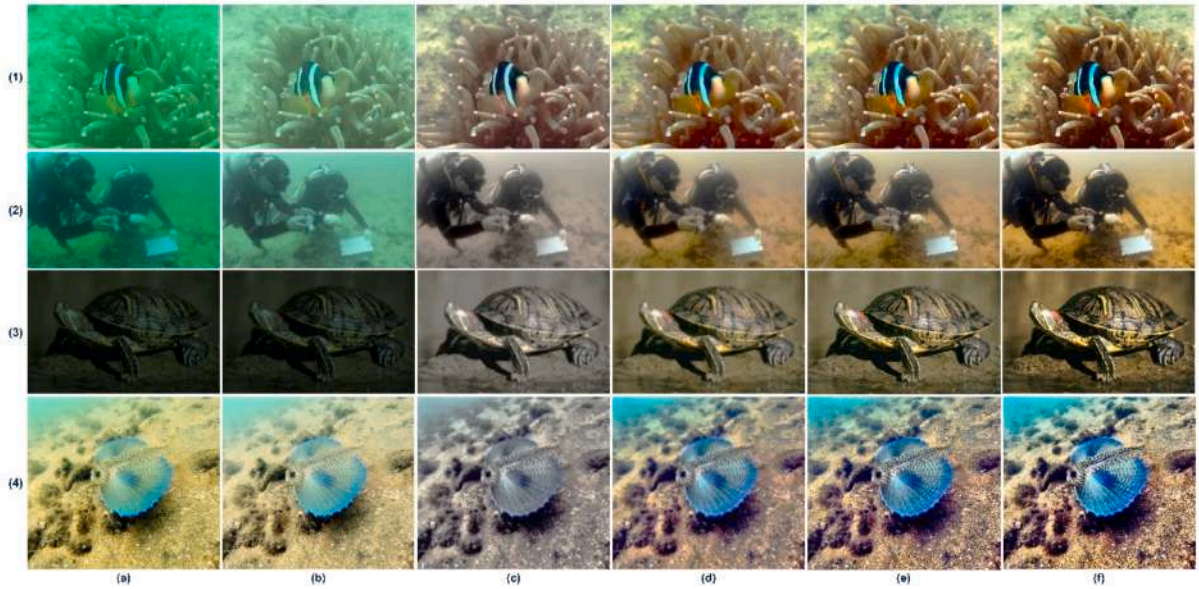

Fig. 13. Subjective comparison of different components of the proposed method on four underwater images. (a) Input image, (b) Proposed CDO, (c) Proposed CDO+GWT, (d) Proposed CDO+GWT+PIS, (e) Proposed CDO+GWT+PIS+GPT, and (f) Proposed CDO+GWT+PIS+GPT+CCE.

and contextual contrast enhancement for underwater image enhancement. The proposed texture enhancement method can effectively improve the quality of underwater images with more realistic textures. A contextual contrast enhancement is formulated for natural color and contrast enhancement without excessive enhancement. Experimental evaluations reveal that the proposed algorithm significantly improves the visibility and perception of underwater scenes and nearly recovers natural colors. In comparison with existing underwater enhancement, our algorithm achieves excellent performance in improving the color and quality of underwater scenes. Extensive experiments on different benchmark data sets show that the proposed method outperforms both qualitative and quantitative metrics. Our future work could mainly focus

Table 9
Objective measurements of different components of the proposed method on four underwater images.

Name	Fish					Man				
Measures	**ENT**	**UIConM**	**UIQM**	**UCIQE**	**BRISQUE**	**ENT**	**UIConM**	**UIQM**	**UCIQE**	**BRISQUE**
Input	7.6208	0.4532	1.1549	0.4190	44.6184	6.7010	0.2966	1.0561	0.4532	40.6348
CDO	7.2356	0.4271	2.1280	0.4124	39.3077	6.3103	0.3324	1.5590	0.4988	35.4799
CDO+GWT	7.4565	0.3620	1.9830	0.5445	36.7015	7.6048	0.3947	3.3877	0.5394	30.3862
CDO+GWT+PIS	7.4455	0.3801	2.1556	0.5963	30.7371	7.6468	0.4046	3.6409	0.6144	29.1069
CDO+GWT+PIS+ GPT	7.3811	0.5597	3.4990	0.6123	28.2550	7.5107	0.6150	3.9686	0.6246	28.7946
CDO+GWT+PIS+ GPT+CCE	**7.7284**	**0.8518**	**5.5790**	**0.6670**	**20.1150**	**7.8344**	**0.8737**	**5.6375**	**0.6583**	**18.3496**
Name	**Turtle**					**Gurnard**				
Input	5.9360	0.6782	4.1382	0.4073	42.7007	7.7161	0.7721	4.6410	0.6017	37.1935
CDO	5.2641	0.6803	4.1910	0.4527	38.4895	6.4683	0.7668	4.6863	0.5376	31.7077
CDO+GWT	6.8460	0.5087	3.6688	0.4855	36.9236	7.2299	0.6438	4.1799	0.5373	34.0562
CDO+GWT+PIS	7.1027	0.5418	3.8720	0.5228	32.0548	7.3616	0.6486	4.2663	0.6085	32.9324
CDO+GWT+PIS+ GPT	7.2743	0.6443	4.4539	0.5633	29.2409	7.3007	0.8207	5.1862	0.6539	18.3501
CDO+GWT+PIS+ GPT+CCE	**7.5227**	**0.8798**	**5.7007**	**0.6714**	**19.9888**	**7.8487**	**0.8282**	**5.7875**	**0.6767**	**17.1935**

on developing a more streamlined implementation for real-time processing and reducing computational time without compromising image quality.

CRediT authorship contribution statement

Bharath Subramani: Project administration, Methodology, Investigation, Funding acquisition, Formal analysis, Data curation, Conceptualization. **Magudeeswaran Veluchamy:** Writing – review & editing, Writing – original draft, Visualization, Validation, Supervision, Software, Resources.

Declaration of competing interest

The authors declare that they have no known competing financial interests or personal relationships that could have appeared to influence the work reported in this paper.

Data availability

Data will be made available on request.

Acknowledgment

The authors declare that there has been no significant financial support for this work.

References

[1] Y. Li, D. Li, Z. Gao, S. Wang, Q. Jiao, L. bian, Underwater image enhancement utilizing adaptive color correction and model conversion for dehazing, Opt. Laser Technol. 169 (2024) 110039, https://doi.org/10.1016/j.optlastec.2023.110039.
[2] C. Dai, M. Lin, X. Wu, Z. Wang, Z. Guan, Single underwater image restoration by decomposing curves of attenuating color, Opt. Laser Technol. 123 (2020) 105947, https://doi.org/10.1016/j.optlastec.2019.105947.
[3] B. Subramani, A.K. Bhandari, M. Veluchamy, Optimal bezier curve modification function for contrast degraded images, in: IEEE Transactions on Instrumentation and Measurement, vol. 70, pp. 1-10, 2021, Art no. 5008910, doi: 10.1109/TIM.2021.3073320.
[4] M. Veluchamy, A.K. Bhandari, B. Subramani, Optimized bezier curve based intensity mapping scheme for low light image enhancement, IEEE Trans. Emerg. Top. Computat. Intell. 6 (3) (June 2022) 602–612, https://doi.org/10.1109/TETCI.2021.3053253.
[5] C.O. Ancuti, C. Ancuti, C. De Vleeschouwer, P. Bekaert, Color balance and fusion for underwater image enhancement, IEEE Trans. Image Process. 27 (1) (Jan. 2018) 379–393, https://doi.org/10.1109/TIP.2017.2759252.
[6] P. Marques, A. Branzan, M. Hoeberechts, A contrast-guided approach for the enhancement of low-lighting underwater images, J. Imaging 5 (79) (2019) 1–24, https://doi.org/10.3390/jimaging5100079.
[7] J. Yuan, W. Cao, Z. Cai, B. Su, An underwater image vision enhancement algorithm based on contour bougie morphology, IEEE Trans. Geosci. Remote Sens. 59 (10) (Oct. 2021) 8117–8128, https://doi.org/10.1109/TGRS.2020.3033407.
[8] S. Wu, et al., A two-stage underwater enhancement network based on structure decomposition and characteristics of underwater imaging, IEEE J. Ocean. Eng. 46 (4) (Oct. 2021) 1213–1227, https://doi.org/10.1109/JOE.2021.3064093.
[9] N. Singh, A.K. Bhandari, Principal component analysis-based low-light image enhancement using reflection model, IEEE Trans. Instrum. Meas. 70 (2021) 1–10, https://doi.org/10.1109/TIM.2021.3096266.
[10] S.-C. Pei, C.-Y. Chen, Underwater images enhancement by revised underwater images formation model, IEEE Access 10 (2022) 108817–108831, https://doi.org/10.1109/ACCESS.2022.3213340.
[11] J. Yuan, Z. Cai, W. Cao, TEBCF: real-world underwater image texture enhancement model based on blurriness and color fusion, IEEE Trans. Geosci. Remote Sens. 60 (2022) 1-15, Art no. 4204315, doi: 10.1109/TGRS.2021.3110575.
[12] R. Kumar, A.K. Bhandari, Fuzzified contrast enhancement for nearly invisible images, IEEE Trans. Circuits Syst. Video Technol. 32 (5) (May 2022) 2802–2813, https://doi.org/10.1109/TCSVT.2021.3098763.
[13] B.P. Kumar, A. Kumar, R. Pandey, Region-based adaptive single image dehazing, detail enhancement and pre-processing using auto-colour transfer method, Signal Process. Image Commun. 100 (2022) 116532, https://doi.org/10.1016/j.image.2021.116532.
[14] S. Wang, Z. Chen, H. Wang, Multi-weight and multi-granularity fusion of underwater image enhancement, Earth Sci. Inf. 15 (2022) 1647–1657, https://doi.org/10.1007/s12145-022-00804-9.
[15] W. Zhang, P. Zhuang, H.-H. Sun, G. Li, S. Kwong, C. Li, Underwater image enhancement via minimal color loss and locally adaptive contrast enhancement, IEEE Trans. Image Process. 31 (2022) 3997–4010, https://doi.org/10.1109/TIP.2022.3177129.
[16] W. Zhang, Y. Wang, C. Li, Underwater image enhancement by attenuated color channel correction and detail preserved contrast enhancement, IEEE J. Ocean. Eng. 47 (3) (July 2022) 718–735, https://doi.org/10.1109/JOE.2022.3140563.
[17] P. Zhuang, J. Wu, F. Porikli, C. Li, Underwater image enhancement with hyper-laplacian reflectance priors, IEEE Trans. Image Process. 31 (2022) 5442–5455, https://doi.org/10.1109/TIP.2022.3196546.
[18] L. Zhou, Q. Liu, Y. Fan, X. Song, X. Pan, W. Zhang, Underwater image enhancement via complementary advantage fusion of global and local contrast, Comput. Electr. Eng. 112 (2023) 108990, https://doi.org/10.1016/j.compeleceng.2023.108990.
[19] X. Sun, Y. Zhu, X. Fu, RGB and optimal waveband image fusion for real-time underwater clear image acquisition, IEEE Trans. Instrum. Measur. 72 (2023) 1-17, Art no. 5019517, doi: 10.1109/TIM.2023.3290366.
[20] F. Xiao, F. Yuan, Y. Huang, E. Cheng, Turbid underwater image enhancement based on parameter-tuned stochastic resonance, IEEE J. Ocean. Eng. 48 (1) (Jan. 2023) 127–146, https://doi.org/10.1109/JOE.2022.3190517.
[21] S. Lu, F. Guan, H. Zhang, H. Lai, Underwater image enhancement method based on denoising diffusion probabilistic model, J. Vis. Commun. Image Represent. 96 (2023) 103926, https://doi.org/10.1016/j.jvcir.2023.103926.
[22] B. Subramani, M. Veluchamy, Cuckoo search optimization-based image color and detail enhancement for contrast distorted images, Color Res. Appl. 47 (4) (2022) 1005–1022, https://doi.org/10.1002/col.22777T.
[23] T. Wang, et al., Underwater image enhancement based on optimal contrast and attenuation difference, IEEE Access 11 (2023) 68538–68549, https://doi.org/10.1109/ACCESS.2023.3292275.
[24] Y. Huang, F. Yuan, F. Xiao, J. Lu, E. Cheng, Underwater image enhancement based on zero-reference deep network, IEEE J. Ocean. Eng. 48 (3) (July 2023) 903–924, https://doi.org/10.1109/JOE.2023.3245686.
[25] Y. Zhang, Q. Jiang, P. Liu, S. Gao, X. Pan, C. Zhang, Underwater image enhancement using deep transfer learning based on a color restoration model, IEEE

J. Ocean. Eng. 48 (2) (2023) 489–514, https://doi.org/10.1109/JOE.2022.3227393.
[26] P. Zhu, Y. Liu, Y. Wen, M. Xu, X. Fu, S. Liu, Unsupervised underwater image enhancement via content-style representation disentanglement, Eng. Appl. Artif. Intel. 126 (2023) 106866, https://doi.org/10.1016/j.engappai.2023.106866.
[27] J. Liu, R.W. Liu, J. Sun, T. Zeng, Rank-one prior: real-time scene recovery, IEEE Trans. Pattern Anal. Mach. Intell. 45 (7) (2023) 8845–8860, https://doi.org/10.1109/TPAMI.2022.3226276.
[28] C. Liu, X. Shu, D. Xu, J. Shi, GCCF: a lightweight and scalable network for underwater image enhancement, Eng. Appl. Artif. Intel. 128 (2024) 107462, https://doi.org/10.1016/j.engappai.2023.107462.
[29] S. Zhang, S. Zhao, D. An, D. Li, R. Zhao, LiteEnhanceNet: A lightweight network for real-time single underwater image enhancement, Expert Syst. Appl. 240 (2024) 122546, https://doi.org/10.1016/j.eswa.2023.122546.
[30] D. Zhang, C. Wu, J. Zhou, W. Zhang, Z. Lin, K. Polat, F. Alenezi, Robust underwater image enhancement with cascaded multi-level sub-networks and triple attention mechanism, Neural Netw. 169 (2024) 685–697, https://doi.org/10.1016/j.neunet.2023.11.008.
[31] J. Yang, J. Wang, Underwater image enhancement method based on golden jackal optimization, Opt. Commun. 552 (2024) 130064, https://doi.org/10.1016/j.optcom.2023.130064.
[32] C. Park, I. Eom, Underwater image enhancement using adaptive standardization and normalization networks, Eng. Appl. Artif. Intell. 127(Part A) (2024) 107445, Doi: 10.1016/j.engappai.2023.107445.
[33] Y. Li, D. Li, Z. Gao, S. Wang, Q. Jiao, L. bian, Underwater image enhancement utilizing adaptive color correction and model conversion for dehazing, Opt. Laser Technol. 169 (2024) 110039, 2024, Doi: 10.1016/j.optlastec.2023.110039.
[34] S. An, L. Xu, Z. Deng, H. Zhang, HFM: a hybrid fusion method for underwater image enhancement, Eng. Appl. Artif. Intel. 127 (2024) 107219, https://doi.org/10.1016/j.engappai.2023.107219.
[35] M. Veluchamy, B. Subramani, Brain tissue segmentation for medical decision support systems, J. Ambient Intell. Hum. Comput. 12 (2021) 1851–1868, https://doi.org/10.1007/s12652-020-02257-8.
[36] A.K. Bhandari, B. Subramani, M. Veluchamy, Multi-exposure optimized contrast and brightness balance color image enhancement, Digital Signal Process. 123 (2022) 103406, https://doi.org/10.1016/j.dsp.2022.103406.
[37] G. Hou, Y. Li, H. Yang, K. Li, Z. Pan, UID2021: an underwater image dataset for evaluation of no-reference quality assessment metrics, ACM Trans. Multimed. Comput. Commun. Appl. 19 (4) (July 2023) 1–14, https://doi.org/10.1145/3578584G.
[38] Q. Jiang, Y. Zhang, F. Bao, X. Zhao, C. Zhang, P. Liu, Two-step domain adaptation for underwater image enhancement, Pattern Recogn. 122 (2022) 108324, https://doi.org/10.1016/j.patcog.2021.108324.
[39] X. Shen, X. Sun, H. Wang, X. Fu, Multi-dimensional, multi-functional and multi-level attention in YOLO for underwater object detection, Neural Comput. & Applic. 35 (2023) 19935–19960, https://doi.org/10.1007/s00521-023-08781-w.
[40] X. Shen, H. Wang, T. Cui, Z. Guo, X. Fu, Multiple information perception-based attention in YOLO for underwater object detection, Vis. Comput. 40 (2024) 1415–1438, https://doi.org/10.1007/s00371-023-02858-2.
[41] H. Wang, M. Yao, G. Jiang, Z. Mi, X. Fu, Graph-Collaborated Auto-Encoder Hashing for Multiview Binary Clustering, IEEE Trans. Neural Netw. Learn. Syst. doi: 10.1109/TNNLS.2023.3239033.
[42] H. Wang et al., Manifold-based incomplete multiview clustering via Bi-consistency guidance, IEEE Trans. Multimed. doi: 10.1109/TMM.2024.3405650.